Interuniversity Master in Nuclear Physics

STUDY OF ^{6}LI WITH THE RODEO ALGORITHM FOR A QUANTUM COMPUTER

Alèxia Martorell Granollers

Supervised by:
Antonio Márquez, Javier Menéndez, Arnau Rios

UNIVERSITAT DE BARCELONA

Contents

Chapter 1

Brief introduction to quantum computing

Nowadays, quantum computing is of great interest because of its advantages over classical computing due to its potential to overcome current classical supercomputers in the simulation of many-body systems. Next, we will explore the key distinctions between the components employed in quantum computing and classical computing.

1.1 Basic of quantum computing

In classical computing, the bit is used as the main element, which can be either in state 0 or in state 1. In quantum computing, however, the main element is the quantum bit or qubit. The qubit, unlike the classical bit, corresponds to a linear combination between two states, state $|0\rangle$, and state $|1\rangle$ [1]

$$|\psi\rangle = \alpha|0\rangle + \beta|1\rangle, \tag{1.1}$$

being $|0\rangle$ and $|1\rangle$ the computational basis states, which are represented as

$$|0\rangle = \begin{bmatrix} 1 \\ 0 \end{bmatrix} \qquad |1\rangle = \begin{bmatrix} 0 \\ 1 \end{bmatrix}. \tag{1.2}$$

In this manner, a qubit can be found in a continuum set of possible states between $|0\rangle$ and $|1\rangle$.

In the case of bits, we can easily determine whether they are in state 0 or 1 by examining them, and the measurement always yields a definite result with a probability of 1. However, the situation is different for qubits. According to the principles of quantum mechanics, measurements of qubits involve a probabilistic aspect. When we measure a qubit, it can collapse into either the state $|0\rangle$ or the state $|1\rangle$ with probabilities of $|\alpha|^2$ and $|\beta|^2$ respectively. In this manner, α and β have to satisfy

$$|\alpha|^2 + |\beta|^2 = 1. \tag{1.3}$$

Given the normalization condition of Eq. (1.3), we can write a qubit state as follows, ignoring a $\exp{(i\gamma)}$ factor that represents a global phase of the state $|\psi\rangle$ which is irrelevant for the measurement,

$$|\psi\rangle = \cos\left(\frac{\theta}{2}\right)|0\rangle + \exp{(i\varphi)}\sin\left(\frac{\theta}{2}\right)|1\rangle. \tag{1.4}$$
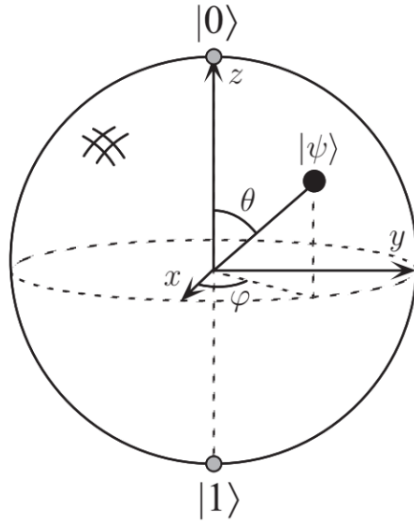
Figure 1.1: Bloch sphere, obtained from [1]. Every qubit, Eq. (1.1), represented by angles θ, φ, Eq. (1.4), corresponds to a vector in a coordinate space (with axes x, y, z) with origin in the center of the sphere and end on its surface.

Hence, to visualize them geometrically, we can represent with a sphere, called Bloch sphere, all the possible states of a qubit in terms of the parameters θ and φ, to visualize them geometrically. Fig. (1.1) represents the Bloch sphere.

In the case that we had two bits in a classic computer, we would have four possible states: 00, 01, 10, and 11. Likewise, in the case of having a two-qubit system, it can be written as a superposition

$$|\psi\rangle = \alpha_{00}|00\rangle + \alpha_{01}|01\rangle + \alpha_{10}|10\rangle + \alpha_{11}|11\rangle, \tag{1.5}$$

with $|00\rangle$, $|01\rangle$, $|10\rangle$, and $|11\rangle$ the computational basis state of two qubits. Analogously to the case of having only one qubit, when we measure the state of the two qubits system, we will obtain one of the computational basis states with a probability of $|\alpha_{00}|^2$, $|\alpha_{01}|^2$, $|\alpha_{10}|^2$ and $|\alpha_{11}|^2$ respectively, with the normalization condition,

$$|\alpha_{00}|^2 + |\alpha_{01}|^2 + |\alpha_{10}|^2 + |\alpha_{11}|^2 = 1. \tag{1.6}$$

Furthermore, in a two-qubit system, it is possible to measure the state of one of the qubits. For example, measuring the first qubit we obtain $|0\rangle$ with a probability

$$P_{q_1 \to |0\rangle} = |\alpha_{00}|^2 + |\alpha_{01}|^2, \tag{1.7}$$

and we obtain $|1\rangle$ with a probability

$$P_{q_1 \to |1\rangle} = |\alpha_{10}|^2 + |\alpha_{11}|^2. \tag{1.8}$$

In the case that we observe $|0\rangle$, the remaining state corresponds to the superposition

$$|\psi'\rangle = \frac{\alpha_{00}|00\rangle + \alpha_{01}|01\rangle}{\sqrt{|\alpha_{00}|^2 + |\alpha_{01}|^2}}. \tag{1.9}$$

In contrast, if we measure for the first qubit the state $|1\rangle$, the state of two qubits will collapse to

$$|\psi''\rangle = \frac{\alpha_{10}|10\rangle + \alpha_{11}|11\rangle}{\sqrt{|\alpha_{10}|^2 + |\alpha_{11}|^2}}, \tag{1.10}$$

since the states after measurement have to be normalized.

After measuring the first qubit, we have the option to perform a second measurement on the second qubit. For example, if we observe the state $|1\rangle$ on the first qubit, which occurs with a probability of Eq. (1.8), and subsequently have the state $|\psi''\rangle$, the probability of obtaining the state $|0\rangle$ on the second qubit is given by

$$P_{q2 \to |0\rangle} = \frac{|\alpha_{10}|^2}{|\alpha_{10}|^2 + |\alpha_{11}|^2}. \tag{1.11}$$

By multiplying these probabilities, Eq. (1.8) and Eq. (1.11), we can recover the probability of obtaining the state $|10\rangle$, which is $|\alpha_{10}|^2$.

Therefore, we can extend this concept to systems with multiple qubits. If we have n_q qubits, the system corresponds to 2^{n_q} computational basis states, resulting in an exponential increase of the number of the classical states with a linear increase in the number of quantum qubits. As a result, in a quantum computer, even with a small number of qubits, we can access states that would require a large number of classical bits in a classical computer. This fundamental characteristic of quantum computing provides a significant advantage over classical computing when it comes to information storage.

1.2 Quantum gates

In the case of classical computing, logic gates are used to manipulate information. For a single bit, there is the NOT gate as an example. A NOT gate acts on a bit that is at 0, it will become 1, but if it was at 1 it will become 0. In quantum computing, analogously, there is a gate that changes the states $|0\rangle$ for $|1\rangle$ and $|1\rangle$ for $|0\rangle$, so if we have a qubit in an arbitrary state such as the expression in Eq. (1.1), after passing through the gate, the qubit is transformed into the state

$$X|\psi\rangle = \alpha|1\rangle + \beta|0\rangle. \tag{1.12}$$

This gate, represented as X, can be defined as an operator, which can be written as a matrix in the computational states basis on a single qubit as

$$X \equiv \begin{bmatrix} 0 & 1 \\ 1 & 0 \end{bmatrix}, \tag{1.13}$$

and fulfills

$$X \begin{bmatrix} \alpha \\ \beta \end{bmatrix} = \begin{bmatrix} \beta \\ \alpha \end{bmatrix}. \tag{1.14}$$

There are different gates, mapped into quantum mechanics operators, that act on a single qubit and can be represented by 2×2 matrices. To maintain the normalization condition, Eq. (1.3), which guarantees the conservation of probability, operators must be unitary, so they must meet the following condition:

$$U^\dagger U = \mathbb{I}, \tag{1.15}$$

with U an arbitrary operator and $\mathbb{I}$ the identity matrix, in the same dimensions as U.
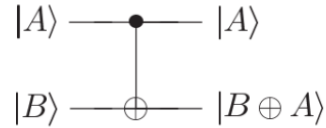
Figure 1.2: Controlled-NOT gate representation, obtained from [1], acting on the two-qubit system $|AB\rangle$. While qubit $|A\rangle$ stays the same, an X gate acts on qubit $|B\rangle$, since $|A\rangle$ corresponds to the control qubit and $|B\rangle$ to the target qubit.

Two widely used single-qubit gates correspond to the Z gate and the Hadamard gate, H. The operator Z corresponds to

$$Z \equiv \begin{bmatrix} 1 & 0 \\ 0 & -1 \end{bmatrix}, \tag{1.16}$$

which leaves the state $|0\rangle$ untouched and changes the state $|1\rangle$ by $-|1\rangle$,

$$Z \begin{bmatrix} \alpha \\ \beta \end{bmatrix} = \begin{bmatrix} \alpha \\ -\beta \end{bmatrix}. \tag{1.17}$$

The Hadamard gate corresponds to

$$H \equiv \frac{1}{\sqrt{2}} \begin{bmatrix} 1 & 1 \\ 1 & -1 \end{bmatrix}, \tag{1.18}$$

which turns the state $|0\rangle$ into

$$\frac{|0\rangle + |1\rangle}{\sqrt{2}}, \tag{1.19}$$

and turns the state $|1\rangle$ into

$$\frac{|0\rangle - |1\rangle}{\sqrt{2}}. \tag{1.20}$$

In a general state, the transformation performed by the Hadamard gate can be described as follows

$$H \begin{bmatrix} \alpha \\ \beta \end{bmatrix} = \frac{1}{\sqrt{2}} \begin{bmatrix} \alpha + \beta \\ \alpha - \beta \end{bmatrix}. \tag{1.21}$$

For classical computing, several gates act on multiple bits. The most used are the OR, AND, and XOR gates. For quantum computing, the main multi-qubit gate

Table 1.1: A two-qubit state before (In) and after (Out) applying the CNOT operator.

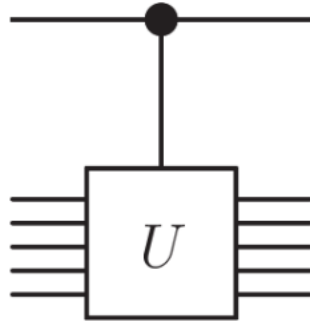| In	Out
$|00\rangle$	$|00\rangle$
$|01\rangle$	$|01\rangle$
$|10\rangle$	$|11\rangle$
$|11\rangle$	$|10\rangle$

Figure 1.3: Controlled-U gate representation, obtained from [1]. The main difference compared to the CNOT gate shown in Fig. (1.2), where there is only one target qubit ($|B\rangle$), is that in this case, the target qubits are represented with multiple lines before and after the U operator. Also, the operator applied is U instead of X.

corresponds to the controlled-NOT (CNOT). Fig. (1.2) represents the action of a CNOT gate on a two-qubit system, one of which corresponds to the control qubit and the other to the target qubit. The control qubit is untouched, while the X operator acts on the target qubit only if the control qubit is on the state $|1\rangle$. Then the transformations are represented in Table 1.1. Considering the first qubit as the control qubit, the CNOT gate can be represented as a matrix:

$$U_{CNOT} = \begin{bmatrix} 1 & 0 & 0 & 0 \\ 0 & 1 & 0 & 0 \\ 0 & 0 & 0 & 1 \\ 0 & 0 & 1 & 0 \end{bmatrix}. \tag{1.22}$$

By applying the H gate and then the CNOT gate to the states of the computational basis of two qubits, we obtain a set of correlated states known as the Bell states. These states hold great significance in the field of quantum computation due to their various applications, one of which involves using them in circuits for quantum state teleportation. The different Bell states are given in Table 1.2.

Likewise, one can build a generalized multi-qubit controlled-U gate, represented in Fig (1.3), with U being any operator applicable to a qubit. In this way, the

Table 1.2: Computational basis states (first column) and the Bell states (second column) resulting from applying the Hardmard and the CNOT gate to the computational basis states.

In (computational)	Out (Bell)
$|00\rangle$	$\frac{|00\rangle+|11\rangle}{\sqrt{2}} \equiv |\beta_{00}\rangle$
$|01\rangle$	$\frac{|01\rangle+|10\rangle}{\sqrt{2}} \equiv |\beta_{01}\rangle$
$|10\rangle$	$\frac{|00\rangle-|11\rangle}{\sqrt{2}} \equiv |\beta_{10}\rangle$
$|11\rangle$	$\frac{|01\rangle-|10\rangle}{\sqrt{2}} \equiv |\beta_{11}\rangle$

controlled-U operator applied on a system of qubits can be written as

$$U_{CU} = \begin{bmatrix} \mathbb{I} & 0 \\ 0 & U \end{bmatrix}.$$

(1.23)

This gate leaves the first qubit corresponding to the control qubit invariant while applying the U operator to the target qubits if the control qubit is in the state $|1\rangle$. Finally, to represent the measurement of a qubit, we use a meter symbol as shown in Fig. (1.4).

Figure 1.4: Quantum circuit symbol for single qubit measurement, obtained from [1]. The two lines after measurement refer to a bit and not a qubit, since the state has collapsed, with M being the measured state.

1.3   Quantum circuits and algorithms

A quantum circuit is constructed using a collection of gates, which are depicted on separate lines. Each line corresponds to a different qubit that needs to be prepared. It is important to note that the circuit is read from left to right, indicating the temporal progression. Furthermore, every circuit includes at least one measurement, as measurements are necessary to extract physical information from the system. In nowadays implementations, the initial state preparation involves cooling atoms to their motional ground state and hyperfine ground state [1].

One of the primary objectives of quantum computing is to explore and create new algorithms that surpass the capabilities of classical algorithms. In recent years, an algorithm called the Variational Quantum Eigensolver (VQE) has been developed using quantum circuits [2]. VQE utilizes the variational principle, using an ansätze and classical optimization [3], to compute the ground state energy of a given Hamiltonian. This kind of problem is important in various physical applications like to mimic the complexity of the internucleon interactions [4] or show ^{24}O as the drip line nucleus of the oxygen chain [5]. Subsequently, other more sophisticated algorithms have been developed, such as the ADAPT-VQE algorithm [6].

Most recently, an innovative algorithm called the rodeo algorithm has emerged, offering a significant advancement in quantum computing. Unlike other variational-based algorithms that are limited to finding only the ground state energy or the first excited state [7], the rodeo algorithm can be used to find all the eigenenergies of a quantum system [8]. This is a major advance considering the importance of finding excited states in nuclear physics [9]. In addition, with this algorithm, information can also be obtained on the corresponding squared amplitudes, probabilities, of each of the eigenvectors in a reference state considered, which can give us information about the nuclear structure and transitions, in case we deal with realistic nuclear systems. Therefore, this algorithm can be very useful, among other branches, for the study of nuclear physics.

The rodeo algorithm involves the preparation of a quantum state and the determination of an energy spectrum to identify eigenenergies within that spectrum, as well as the probabilities of measuring these eigenenergies for the reference state. This is done by filtering the state [10]. Unlike traditional quantum algorithms, the rodeo algorithm incorporates temporal evolution along with auxiliary qubits called ancilla qubits [11]. Initial testing of the rodeo algorithm has been carried out using simple Hamiltonians like the Heisenberg model. However, our work focuses on applying this algorithm to a realistic Hamiltonian for the ^{6}Li nucleus, opening up new possibilities for the study of nuclear physics.

In the following sections, we present a theoretical framework for the rodeo circuit. Our objective is to conduct a detailed study to determine the optimal parameters required in the circuit, minimizing computational effort while obtaining the desired energies and probabilities. Additionally, we have developed an algorithm specifically designed to identify both the eigenenergies and probabilities of interest for a specific state and Hamiltonian, focusing on the case of ^{6}Li nuclei. We use a phenomenological state-of-the-art Hamiltonian that describes ^{6}Li well within the framework of the nuclear shell model. By comparing the results obtained with our implementation of the rodeo algorithm with the exact values obtained by the diagonalization of the Hamiltonian, we aim to validate the effectiveness and accuracy of our algorithm.

Chapter 2

Rodeo Algorithm

In this chapter, we introduce the rodeo circuit, which encompasses a set of gates along with their corresponding functions. Furthermore, we derive probability expressions for the expected results of the measurements of the qubits involved, that enable us to examine how these probabilities change in response to the various parameters employed within the circuit. The primary objective of the circuit is to determine the eigenenergies of the Hamiltonian of a system, based on filtering the possible results of an energy measurement of a given reference state. The circuit is designed to manipulate the quantum state in such a way that it provides insight into the eigenenergies of interest, enabling us to study and analyze the energy spectrum of the system.

2.1 Rodeo circuit

Fig. (2.1) shows the general diagram of the rodeo circuit. The circuit requires N ancilla qubits, all of them in the state $|1\rangle$, in addition to an initial or reference state $|\psi_I\rangle$, which can be decomposed into eigenstates of the Hamiltonian of which we would like to obtain its eigenvalues. The auxiliary qubits are additional qubits used in the circuit that do not correspond to any specific physical state of study. They serve as intermediate computational resources to enable certain quantum operations or transformations within the circuit. Initially to each of the ancilla qubits, we apply the Hardmard gate, which consists of applying the operator H, given in matrix form in Eq. (1.18).

Then, the controlled-U gate is applied to the subspace of the first ancilla qubit and the $|\psi_I\rangle$ state ($|1\rangle \otimes |\psi_I\rangle$), where U is the time evolution operator, $\exp(-iH_{obj}t_1)$, H_{obj} the Hamiltonian of the system state $|\psi_I\rangle$, and t_1 the time at which the time evolution operator is applied. This gate is equivalent to making the time operator act to the $|\psi_I\rangle$ state, only if the ancilla qubit is in state $|1\rangle$, so it is equivalent to the operator

$$\exp(-iH_{obj}t_1)\left[|1\rangle \otimes |\psi_I\rangle\right] = \begin{bmatrix} \mathbb{I} & 0 \\ 0 & \exp(-iH_{obj}t_1) \end{bmatrix}, \qquad (2.1)$$

where $\mathbb{I}$ is the identity matrix, in the same dimensions as state $|\psi_I\rangle$, and we use $\hbar = 1$. To maintain consistency with the units of energy, we will express the times t_n in units obtained by dividing $\hbar$ by the units we are using for energy. Next, the phase rotation gate, $P(Et_1)$, is applied to the same ancilla qubit. This corresponds
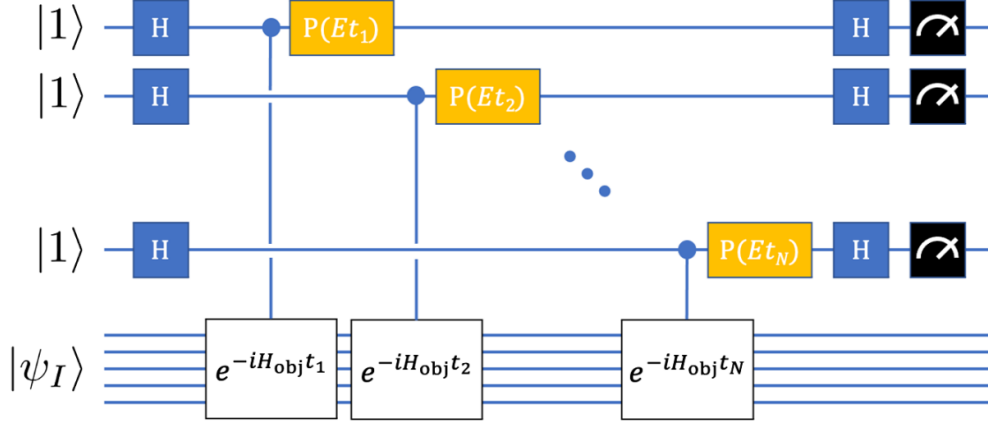
Figure 2.1: Rodeo algorithm circuit, obtained from [8]. For a detailed explanation of all parts of the circuit see the text.

to multiplying by the phase $\exp\left(iEt_1\right)$ if the qubit is in the state $|1\rangle$ and leaving the qubit untouched if it is in the state $|0\rangle$. Here the E parameter, corresponding to energy values, is appropriately chosen by us. Thus, the operator acting on the subspace of the first ancilla qubit and the state $|\psi_I\rangle$ ($|1\rangle \otimes |\psi_I\rangle$) corresponds to

$$P(Et_1)\left[|1\rangle \otimes |\psi_I\rangle\right] = \begin{bmatrix} \mathbb{I} & 0 \\ 0 & \exp\left(iEt_1\right) \end{bmatrix}. \tag{2.2}$$

In the rodeo circuit, the same operations are applied to each ancilla qubit using the individual time t_n, with each time corresponding to a distinct rodeo cycle. Following these operations, the circuit applies the Hadamard gate to each ancilla qubit and then measures their states.

The initial subspace before measuring the ancilla qubits, $|1\rangle \otimes |\psi_I\rangle$, after applying the aforementioned gates, corresponds to the entangled state resulting from the combined operations on the ancilla qubits and the initial state $|\psi_I\rangle$:

$$|1\rangle \otimes |\psi_I\rangle \xrightarrow{Rodeo}$$

$$\frac{1}{\sqrt{2}} \begin{bmatrix} 1 & 1 \\ 1 & -1 \end{bmatrix} \begin{bmatrix} \mathbb{I} & 0 \\ 0 & \exp\left(iEt_n\right) \end{bmatrix} \begin{bmatrix} \mathbb{I} & 0 \\ 0 & \exp\left(-iH_{obj}t_n\right) \end{bmatrix} \frac{1}{\sqrt{2}} \begin{bmatrix} 1 & 1 \\ 1 & -1 \end{bmatrix} \begin{bmatrix} 0 \\ |\psi_I\rangle \end{bmatrix} \tag{2.3}$$

$$= \begin{bmatrix} \left(\frac{\mathbb{I}}{2} - \frac{1}{2}\exp\left(-it_n[H_{obj} - E]\right)\right)|\psi_I\rangle \\ \left(\frac{\mathbb{I}}{2} + \frac{1}{2}\exp\left(-it_n[H_{obj} - E]\right)\right)|\psi_I\rangle \end{bmatrix}.$$

Therefore, the probability that an ancilla qubit n is in state $|1\rangle$, represented as P_n, is

$$P_n = \langle\psi_I| \left|\left(\frac{\mathbb{I}}{2} + \frac{1}{2}\exp\left(-it_n[H_{obj} - E]\right)\right)\right|^2 |\psi_I\rangle$$

$$= \langle\psi_I| \cos^2\left(\frac{t_n(H_{obj} - E)}{2}\right)|\psi_I\rangle, \tag{2.4}$$

corresponding to the conjugate product of the projected resultant state in the state of ancilla qubit $|1\rangle$. Writing the state $|\psi_I\rangle$ in the eigenvector basis H_{obj}, we arrive

at the following expression

$$P_n = \sum_i c_i{}^2 \cos^2 \left(\frac{t_n(E_{obj\,i} - E)}{2} \right), \tag{2.5}$$

being c_i the projections of the $|\psi_I\rangle$ state on each eigenvector,

$$|\psi_I\rangle = \sum_i c_i |E_{obj\,i}\rangle, \tag{2.6}$$

and $E_{obj\,i}$ the eigenvalues of H_{obj},

$$H_{obj}|E_{obj1}\rangle = E_{obj\,i}|E_{obj1}\rangle, \tag{2.7}$$

where i runs through all H_{obj} eigenvalues. After N_C rodeo cycles, corresponding to considering the evolution of N_C ancilla qubits with the initial state $|\psi_I\rangle$, the final state just before measuring each ancilla qubit and projecting all the ancilla qubits onto the state $|1\rangle$, can be expressed as:

$$\langle 1| \otimes \dots \otimes \langle 1| \otimes \mathbb{I} \left[|1\rangle \otimes \dots \otimes |1\rangle |\psi_I\rangle \xrightarrow{Rodeo} \right]$$
$$\left(\frac{\mathbb{I}}{2} + \frac{1}{2}\exp{-it_1[H_{obj} - E]} \right) \dots \left(\frac{\mathbb{I}}{2} + \frac{1}{2}\exp{-it_{N_C}[H_{obj} - E]} \right) |\psi_I\rangle. \tag{2.8}$$

Thus, the probability that N_C ancilla qubits are in state $|1\rangle$, represented as P_{N_C}, corresponds therefore to

$$P_{N_C} = \langle\psi_I| \prod_{n=1}^{N_C} \cos^2 \left(\frac{t_n(H_{obj} - E)}{2} \right) |\psi_I\rangle, \tag{2.9}$$

and in the eigenvector basis of H_{obj}, it corresponds to

$$P_{N_C} = \sum_i c_i{}^2 \prod_{n=1}^{N_C} \cos^2 \left(\frac{t_n(E_{obj\,i} - E)}{2} \right). \tag{2.10}$$

Considering Eq. (2.10), we can anticipate that the probability of obtaining all ancilla qubits in the $|1\rangle$ state, denoted as P_{N_C}, will be proportional to the square of the coefficient $P_{N_C} = c_i^2$ when the energy is one of the eigenenergies $E = E_{obj\,i}$, since the maximum value of the cosine is one. Furthermore, as we move away from the eigenenergies, the probability of obtaining all ancilla qubits in the $|1\rangle$ state is expected to decrease.

In a quantum computer, rather than dealing with probability expressions directly, we measure the final state of the ancilla qubits. Based on this measurement, we can calculate the probability of obtaining all the ancilla qubits in the state $|1\rangle$ by dividing the number of ancilla qubits observed in the state $|1\rangle$ by the total number of ancilla qubits, N_C.

When dealing with a small number of ancilla qubits, this approach provides limited information. To mitigate this limitation, we can perform the rodeo cycle multiple times, N_C, and average the probabilities obtained. For example, if we consider three cycles of the rodeo circuit and perform the circuit once, we may

observe 0, 1, 2, or 3 ancilla qubits in the state $|1\rangle$. Consequently, the resulting probabilities obtained using this single measurement would be 0, $\frac{1}{3}$, $\frac{2}{3}$, or 1.

To obtain more accurate probabilities, we can repeat the circuit multiple times, N_{av}, with the same number of cycles and average the probabilities obtained from each run. By increasing the number of repetitions, we can obtain a more reliable estimation of the probabilities associated with the desired outcome.

2.2 Analysis of rodeo algorithm

To effectively implement the rodeo algorithm on a quantum computer, it is crucial to optimize the circuit parameters. This optimization serves to improve result accuracy and reduce computational effort. In the upcoming sections, we explore the impact of various timing configurations on the performance of the rodeo circuit. By studying and analyzing different timing schemes, we aim to identify strategies that enhance the circuit's efficiency and overall effectiveness.

To begin the analysis of the rodeo algorithm, let us consider a simple Hamiltonian in arbitrary units (A.U.), represented by 2×2 matrix, that we use throughout the section, as an example:

$$H_{obj} = \begin{bmatrix} 4 & -1 \\ -1 & 3 \end{bmatrix}. \tag{2.11}$$

The choice of a symmetric matrix is significant because it corresponds to a real Hamiltonian since in quantum mechanics, physical observables are represented by Hermitian operators, which have real eigenvalues. This Hamiltonian has two eigenvalues, $\lambda_{\pm} = \frac{7 \pm \sqrt{5}}{2}$, $\lambda_1 \simeq 4.618$, $\lambda_2 \simeq 2.382$, that we find by diagonalizing the matrix. By doing so we also obtain the eigenvectors.

2.2.1 Choice of times t_n

Eq. (2.10) indicates that the probability of obtaining the state $|1\rangle$ in N_C ancilla qubits depends on the times, t_n, associated with the time evolutions of the Hamiltonian and the phase rotation in each rodeo cycle. As an initial approach, we can employ a constant time throughout the entire rodeo cycle.

Constant times

First, we choose for the $|\psi_I\rangle$ reference state each of the eigenvectors of the Hamiltonian in Eq. (2.11) and calculate the probability of obtaining $|1\rangle$ in each of the ancilla qubits considered by taking different numbers of cycles, N_C, for different energy values E. Fig. (2.2) shows the probabilities of finding all the states of the ancilla qubits $|1\rangle$ for different energies, for each of the eigenvectors of the Hamiltonian, Eq. (2.11). For each color, and therefore for each eigenvector, we expect to find a probability of 1, $P_{N_C} = 1$, when the energy is the eigenenergy, and we expect to see it decrease as we move away from the eigenenergy, so we expect to see only one peak corresponding to its eigenenergy. However, Fig. (2.2) features more than one peak for each color.

These spurious energy values identified by the rodeo algorithm in Fig. (2.2) can be understood because the expression of the probability, Eq. (2.10), is proportional to a cosine squared. Therefore, in addition to the peak due to the energy corresponding
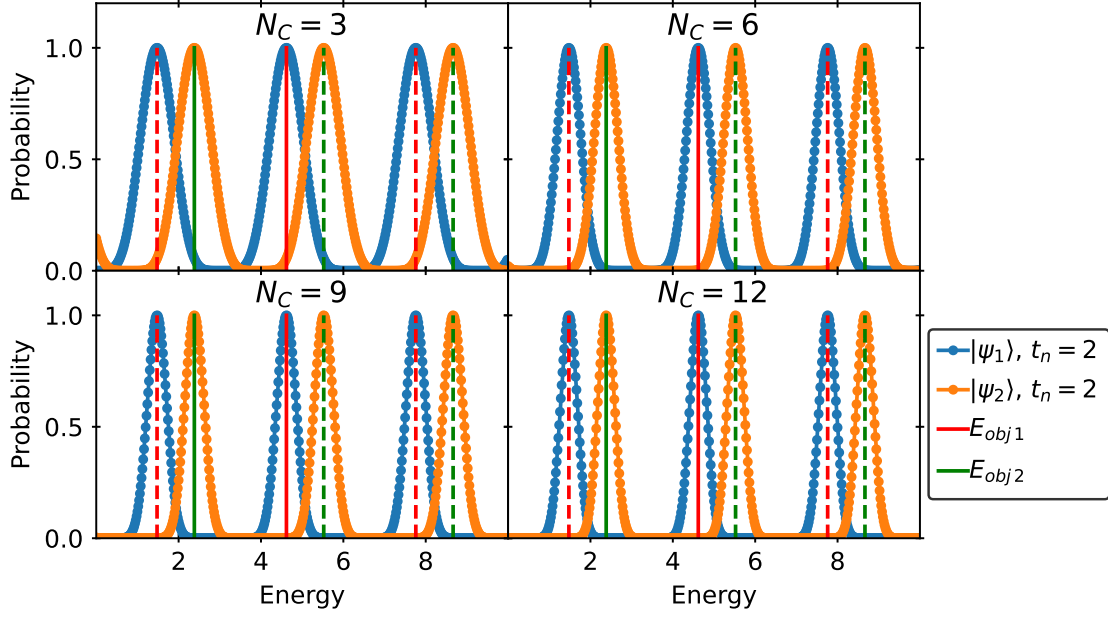
Figure 2.2: Rodeo cycle probability for different number of cycles, $N_C = 3,6,9,12$ as a function of the energies E (in A.U.)., taking as reference the state $|\psi_1\rangle$, the eigenvector associated to $E_{obj1} \simeq 4.618$ (blue) and $|\psi_2\rangle$, the eigenvector associated to $E_{obj2} \simeq 2.382$ (orange), for the Hamiltonian in Eq. (2.11). The value of the times used for each cycle corresponds to $t_n = 2$. The vertical solid lines correspond to the energy eigenvalues, in red for E_{obj1} and in green for E_{obj2}. The dashed lines correspond to energies associated to each reference state with probability = 1 without being the eigenenergies.

to the eigenenergy, there are other peaks which appear due to the periodicity of the cosine. In fact, for each eigenvector as reference state, the probability of the rodeo cycle is 1, the maximum, for the energies that fulfill the following expressions:

$$
\cos^2 \left(\frac{t_n(E_{obj\,i} - E)}{2} \right) = 1,
$$

$$
\rightarrow E = E_{obj} + \frac{2\pi k}{t_n},
$$

(2.12)

where k is an integer. In Fig. (2.2), the first blue peak is due to the energy $E = E_{obj1} - \pi$ ($k = -1$) represented with a dashed red line. The second peak is due to the eigenenergy $E = E_{obj1}$ ($k = 0$) represented with a solid red line and the third peak is due to the energy $E = E_{obj1} + \pi$ ($k = 1$), represented with a dashed red line, since we have considered $t_n = 2$. Indeed, the probability on a broader energy range shows more peaks corresponding to the different integers k of the Eq. (2.12). Likewise, Fig. (2.2) shows spurious peaks associated with eigenvalue $\lambda_2 = 2.382$, represented by the orange peaks with dashed green lines. The true eigenvalue is given by the orange peak with a solid green line. Fig. (2.2) also highlights that using more cycles of the rodeo algorithm, the peaks become narrower, making it easier to distinguish the maximum probability energies of each peak.

Using a general state as a reference state, as described by Eq. (2.6), which can be expressed in terms of the eigenvector basis, we can expect the rodeo algorithm
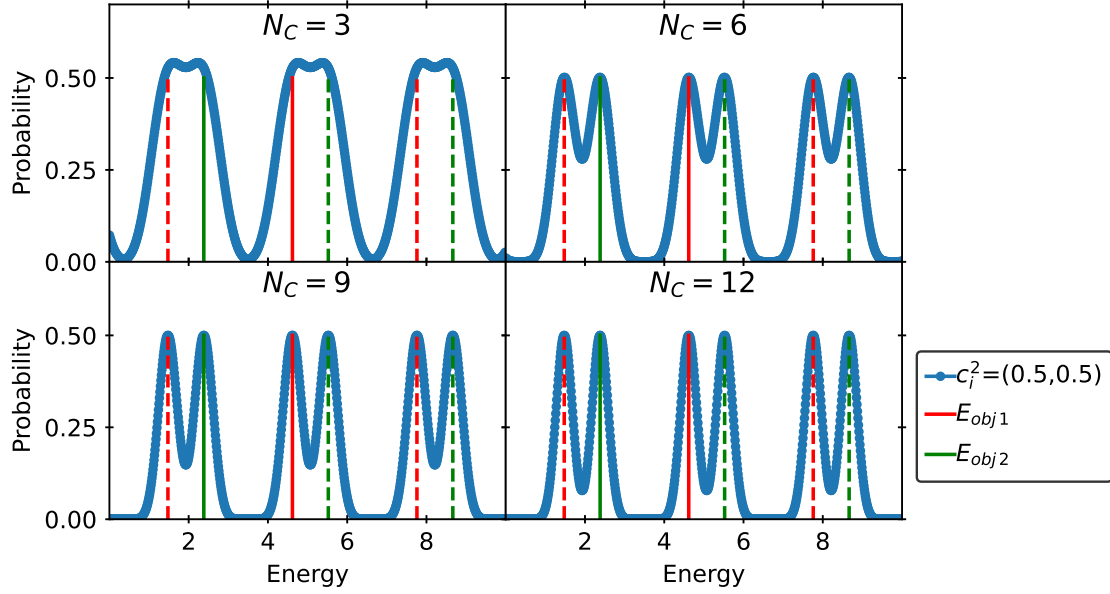
Figure 2.3: Same as Fig. (2.2), but taking the reference state $|\psi_I\rangle = \sqrt{0.5}|E_{obj1}\rangle + \sqrt{0.5}|E_{obj2}\rangle$. The height of the solid lines corresponds to the probability of finding a given eigenenergy when measuring the reference state.

to exhibit peaks in the probability distribution corresponding to each eigenvalue of energy. These peaks are expected to occur around $E_{\text{obj}} \pm \frac{2\pi k}{t_n}$, where k represents an integer and only $k = 0$ corresponds to the true eigenvalue. Figs.(2.3) and (2.4) shows the rodeo probability using a reference state $\psi_I = \sqrt{0.5}|E_{obj\,1}\rangle + \sqrt{0.5}|E_{obj\,2}\rangle$ and $\psi_I = \sqrt{0.9}|E_{obj\,1}\rangle + \sqrt{0.1}|E_{obj\,2}\rangle$, respectively. As anticipated, both figures exhibit the expected behavior, with the maximum probability of each peak is given by c_i^2.

Additionally, we observe in Figs.(2.3) and (2.4) that for a smaller number of cycles, such as $N_C = 3$, it becomes challenging to distinguish closely located peaks as they tend to overlap. This overlap occurs because the peaks become broader when the number of cycles is reduced, as also observed in Fig (2.2). This effect is more pronounced when there are more distinct differences in probabilities, as shown in Fig. (2.4), where only the highest peak is distinguishable due to its significantly higher probability.

Uniform/Gaussian distribution times

To address the issue of spurious peaks caused by using constant times in the rodeo algorithm, we can employ random times instead. By introducing randomness in the timing configurations, we aim to mitigate the undesirable effects and improve the accuracy in identifying the eigenenergies of the Hamiltonian.

We calculate the average probability analytically of obtaining the state $|1\rangle$ on a single ancilla qubit, denoted as n, considering the case where random times are utilized. The analytical expression for this average probability depends on the random time distribution. Thus the expression Eq. (2.5) using the analytical average
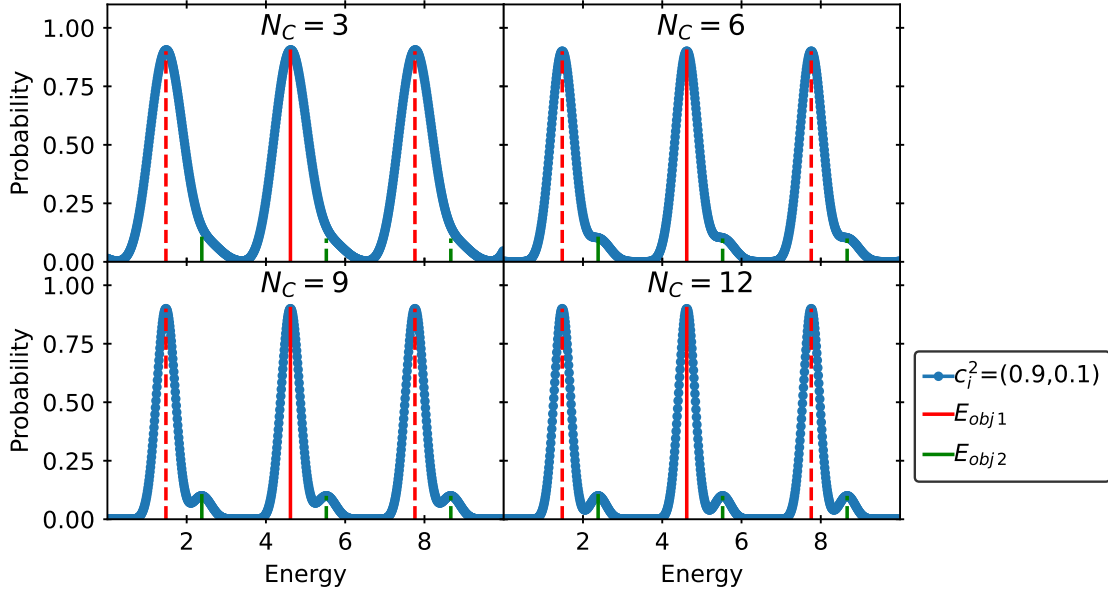
Figure 2.4: Same as Fig. (2.2), but taking the reference state $|\psi_I\rangle = \sqrt{0.9}|E_{obj1}\rangle + \sqrt{0.1}|E_{obj2}\rangle$. The height of the solid lines corresponds to the probability of finding a given eigenenergy when measuring the reference state.

for random numbers takes the expression:

$$
\begin{aligned}
\langle P_n \rangle_{\rho(t_n)} &= \left\langle \sum_i c_i^2 \cos^2 \left(\frac{t_n(E_{obj\,i} - E)}{2} \right) \right\rangle_{t_n \to \rho(t_n)} \\
&= \sum_i c_i^2 \int dt_n \cos^2 \left(\frac{t_n(E_{obj\,i} - E)}{2} \right) \rho(t_n),
\end{aligned}
\tag{2.13}
$$

where $\rho(t)$ is the density function of the probability distribution. The calculation of the average probability of obtaining the state $|1\rangle$ on a single ancilla qubit involves a summation over all eigenenergies and an integral of the squared cosine term, which accounts for the contribution of the random times, with respect to the distribution density of the random numbers at those times. Using a uniform distribution

$$
\rho_U(t_a, t_b) = \frac{1}{t_b - t_a},
\tag{2.14}
$$

where all times between t_a and t_b have the same probability of occurrence, the average probability of obtaining the n qubit ancilla in the state $|1\rangle$ corresponds to:

$$
\langle P_n \rangle_{\rho_U(t_a, t_b)} = \sum_i c_i^2 \frac{1}{2} \left[1 + \frac{\sin\left((E_{obj\,i} - E)t_b\right) - \sin\left((E_{obj\,i} - E)t_a\right)}{(t_b - t_a)(E_{obj\,i} - E)} \right].
\tag{2.15}
$$

Sinusoidal terms appear considering uniform distribution. After N_C cycles of the rodeo algorithm, the probability of obtaining the N_C qubits ancilla in the state $|1\rangle$, considering each cycle independent respect the others, is

$$
\langle P_{N_C} \rangle_{\rho_U(t_a, t_b)} = \sum_i c_i^2 \frac{1}{2^{N_C}} \left[1 + \frac{\sin\left((E_{obj\,i} - E)t_b\right) - \sin\left((E_{obj\,i} - E)t_a\right)}{(t_b - t_a)(E_{obj} - E)} \right]^{N_C}.
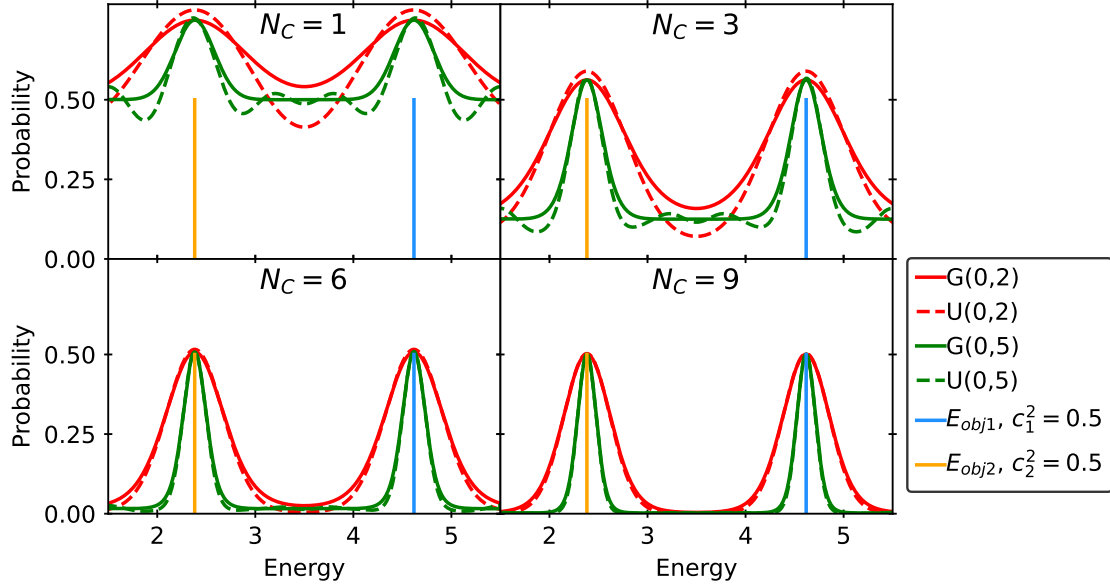\tag{2.16}
$$

Figure 2.5: Rodeo probability average for $N_C = 1, 3, 6$ and 9 rodeo cycles, for different values of energy (in A.U.) taking the reference state $|\psi_I\rangle = \sqrt{0.5}|E_{obj1}\rangle + \sqrt{0.5}|E_{obj2}\rangle$ for the Hamiltonian of Eq. (2.11). Random times are used with uniform distribution $U(\mu, \sigma_t)$ in Eq. (2.14), dashed line, and Gaussian distribution $G(\mu, \sigma_t)$ in Eq. (2.19), solid line. The distributions are centered in $\mu = 0$ for different values of the standard deviation, $\sigma_t = 2$ in red and $\sigma_t = 5$ in green. The vertical solid lines correspond to the energy eigenvalues, in blue for E_{obj1} and in orange for E_{obj2}, and their height represents the probability of measuring such energy for $|\psi_I\rangle$.

Eq. (2.16) is obtained by taking the product of the probabilities for each cycle, corresponding to Eq. (2.15), raised to the power of N_C, given the overall probability of obtaining the desired outcome across all cycles of the rodeo algorithm.

Now taking $t_a = -t_b$ for symmetry, we can rewrite this expression in terms of the standard deviation of the density, $\sigma_t = \sqrt{\int (t - \mu)^2 \rho(t) dt}$, and its average value, $\mu = \int t \rho(t) dt$, with $\mu = 0$ in our case of symmetric initial and final times. The final expression is

$$\langle P_{N_C} \rangle_{\rho_U(0, \sigma_t)} = \sum_i c_i^2 \frac{1}{2^{N_C}} \left[1 + \frac{\sin\left((E_{obj\,i} - E)\sqrt{3}\sigma_t\right)}{(E_{obj\,i} - E)\sqrt{3}\sigma_t} \right]^{N_C}. \quad (2.17)$$

The term $\frac{1}{2^{N_C}}$ represents the initial probability contribution for each eigenstate. Meanwhile, the expression

$$\frac{\sin\left((E_{\{obj\,i} - E)\sqrt{3}\sigma_t\right)}{(E_{obj\,i} - E)\sqrt{3}\sigma_t}, \quad (2.18)$$

incorporates the effect of the energy difference between the eigenvalue $E_{obj\,i}$ and the reference energy E, modulated by the standard deviation σ_t of the random time distribution.

In addition, we calculate also the probability to get the N_C ancilla qubits in the
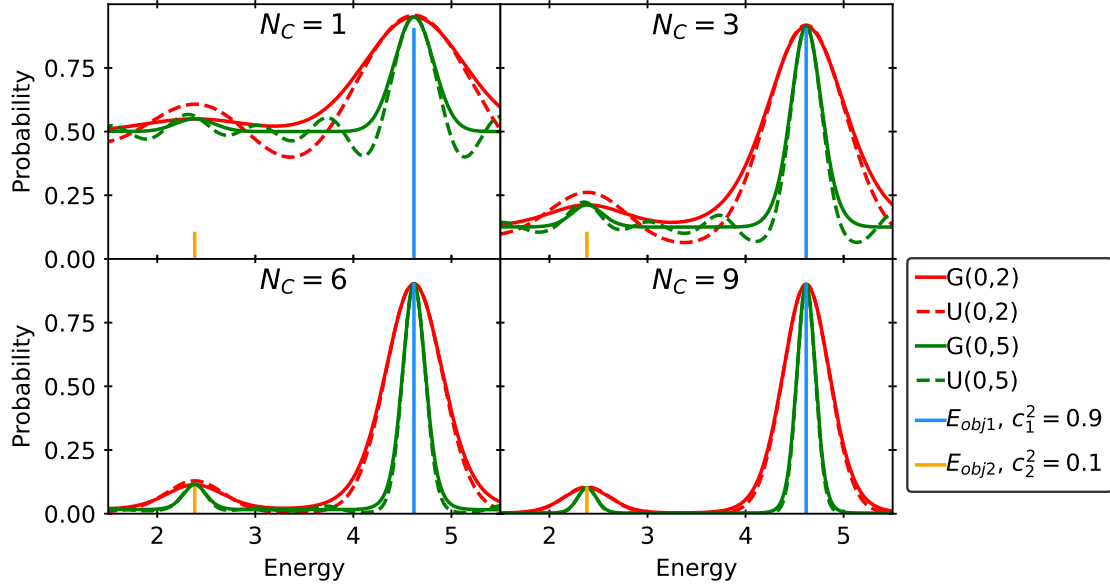
Figure 2.6: Same as Fig. (2.5) but taking taking the reference state $|\psi_I\rangle = \sqrt{0.9}|E_{obj1}\rangle + \sqrt{0.1}|E_{obj2}\rangle$.

state $|1\rangle$, but considering this time a Gaussian distribution:

$$\rho_G(t, \mu, \sigma_t) = \frac{\exp\left(-\frac{(t-\mu)^2}{2\sigma_t^2}\right)}{\sqrt{2\pi}\sigma_t}, \tag{2.19}$$

for the times t_n. We can write the expression in terms of the standard deviation of the density, $\sigma_t = \sqrt{\int (t-\mu)^2 \rho(t)dt}$, and its average value, $\mu = \int t\rho(t)dt$,

$$\langle P_{N_C}\rangle_{\rho_G(\mu,\sigma_t)} = \sum_i c_i^2 \frac{1}{2^{N_C}}\left[1 + \exp\left(-\frac{\sigma_t^2}{2}(E_{obj\,i} - E)^2\right) \cdot \cos\left((E_{obj\,i} - E)\mu)\right)\right]^{N_C}. \tag{2.20}$$

Considering times following a Gaussian distribution, we see that exponential terms appear, instead of the sinusoidal terms that appear when considering a uniform distribution, in Eq. (2.17). Taking also the centered time value $\mu = 0$ for symmetry, we finally obtain:

$$\langle P_{N_C}\rangle_{\rho_G(0,\sigma_t)} = \sum_i c_i^2 \frac{1}{2^{N_C}}\left[1 + \exp\left(-\frac{\sigma_t^2}{2}(E_{obj\,i} - E)^2\right)\right]^{N_C}, \tag{2.21}$$

where the cosine term disappears for this case. The rodeo probability expressions for obtaining N_C ancilla qubits in the state $|1\rangle$ with a uniform distribution of times and a Gaussian distribution of times centered at 0, $\mu = 0$, share similar structures. In the case of a uniform distribution, the probability expression gives rise to sinusoidal behavior. On the other hand, when using a Gaussian distribution, the probability expression involves exponential terms.

Fig. (2.5) and (2.6) illustrate the average probability of obtaining all N_C ancilla qubits in the state $|1\rangle$ using two different reference states: $|\psi_I\rangle = \sqrt{0.5}|E_{obj\,1}\rangle + \sqrt{0.5}|E_{obj\,2}\rangle$ and $|\psi_I\rangle = \sqrt{0.9}|E_{obj\,1}\rangle + \sqrt{0.1}|E_{obj\,2}\rangle$, respectively. The dashed lines
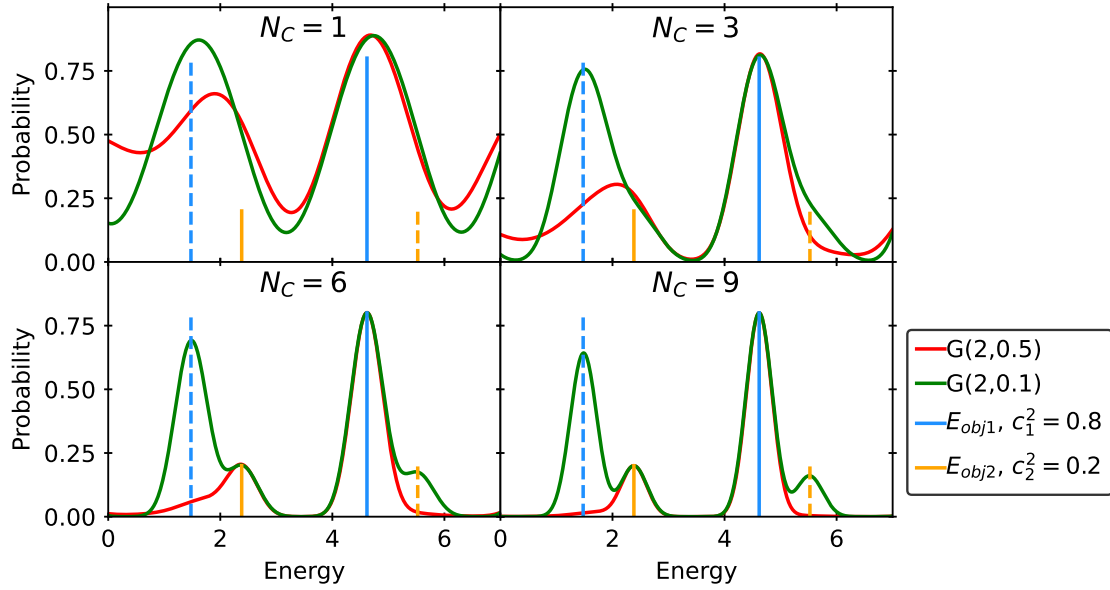
Figure 2.7: Same as Fig. (2.5) but taking taking the reference state $|\psi_I\rangle = \sqrt{0.8}|E_{obj1}\rangle + \sqrt{0.2}|E_{obj2}\rangle$ and using Gaussian distributions with $\mu = 2$ and standard deviation $\sigma_t = 0.5$ (red) and $\sigma_t = 0.1$ (green).

represent the results obtained using a uniform distribution of times (U), while the solid lines depict the results with a Gaussian distribution of times (G). Each color corresponds to a different standard deviation, σ_t, for the distributions.

In both figures, it is evident that additional spurious peaks no longer appear, and the only peaks observed correspond to the eigenenergies. This aligns with the expected behavior based on the derived analytical expressions for the probabilities. For the uniform distribution, the presence of oscillations near the peaks and their absence far from the peaks is consistent with the sinusoidal contribution in the analytical expression, Eq. (2.17). In contrast, the Gaussian distribution exhibits no oscillations due to the exponential nature of the function in the analytical expression, Eq. (2.19), which decays without oscillatory behavior.

The magnitude of these oscillations decreases as the number of cycles increases. Additionally, as for the constant times, the width of the peaks reduces as the number of cycles increases, indicating improved resolution. The width of the peaks is also influenced by the standard deviation σ_t, with narrower peaks observed for larger values of σ_t, as the green peaks ($\sigma_t = 5$) are narrower as the red peaks ($\sigma_t = 2$).

Another important aspect that stands out compared to the case in which the times t_n are constant, is that the average probability is not zero far from the peaks, there is a baseline probability that tends to a constant value. Nonetheless, as the number of rodeo cycles increases, this constant value is closer and closer to zero. Also, we note that the maximum probability of each peak does not correspond exactly to the projection of the state we are considering into each eigenvector of the Hamiltonian, c_i^2, but is overestimated. Again the probability becomes more and more similar to the exact value as the number of cycles increases.

This baseline probability different from zero, combined with the oscillations discussed in the previous paragraph, results in the fact that for a small number of cycles, the oscillations on the average probability using a uniform probability can be

confused with another peak due to an eigenvalue. For this reason, in the following we use random times with a Gaussian distribution for a better resolution.

Gaussian distributed times with small standard deviation

In Fig. (2.7), we present the average probability of obtaining all N_C ancilla qubits in the state $|1\rangle$ using the reference state $|\psi_I\rangle = \sqrt{0.8}|E_{obj\,1}\rangle + \sqrt{0.2}|E_{obj\,2}\rangle$. The probability is calculated with a Gaussian distribution of random times with a small standard deviation and a mean of $\mu = 2$.

We observe the reappearance of additional spurious peaks for the same eigenvalue. This behavior arises due to the random times becoming increasingly close to each other, which effectively simulates the behavior seen with constant times. As the times converge, the probability distribution exhibits peaks that are similar to those observed when using constant times. Therefore, to avoid these spurious states when using a Gaussian distribution for the times t_n, the standard deviation of the distribution needs to be sufficiently large.

To visualize these peaks clearly, in Fig. (2.7) the random times have been centered around $\mu = 2$ units instead of $\mu = 0$. This adjustment is made to prevent the probability from tending towards 1 as the times approach 0, which would make the peaks difficult to discern.

2.2.2 Rodeo algorithm using random Gaussian times

As established in the previous section, Gaussian random times offer a more accurate approach for identifying the eigenenergies of a system compared to uniform random times or constant times. Therefore, in the following sections, we utilize Gaussian random times to achieve more precise results in the rodeo algorithm.

In the context of quantum computing, where the purpose is to determine the eigenenergies of a system, it is important to note that we do not have prior knowledge of these eigenenergies. As a result, we cannot rely on the average probability calculated based on known eigenvalues as we have used in section 2.2.1 for the average of the probabilities following a distribution for random times. Instead, in this section we directly utilize the probability expression, Eq. (2.9), choosing the times using a Gaussian distribution centered at $\mu = 0$.

By employing Gaussian random times centered at $\mu = 0$, we can explore the probability landscape and analyze the behavior of the rodeo algorithm to effectively identify the eigenenergies of the system. This approach allows us to leverage the potential of quantum computing to simulate and solve complex problems related to eigenenergy determination.

In this manner, without an average over the random times we therefore take the following expression as the probability in the rodeo cycle:

$$(P_{N_C})_{t_n \to G(0,\sigma_t)} = \prod_n^{N_C} \sum_i \left[c_i^2 \cos^2\left(\frac{t_n(E_{obj\,i} - E)}{2}\right) \right]_{t_n \to G(0,\sigma_t)}. \tag{2.22}$$

In Fig. (2.8), we represent the probability of obtaining all the ancilla qubits in the state $|1\rangle$ using random times drawn from a Gaussian distribution, as given by Eq. (2.22), for various numbers of rodeo cycles considered in the circuit. In the Figure, an eigenvector has been taken as a state to observe only one peak. The
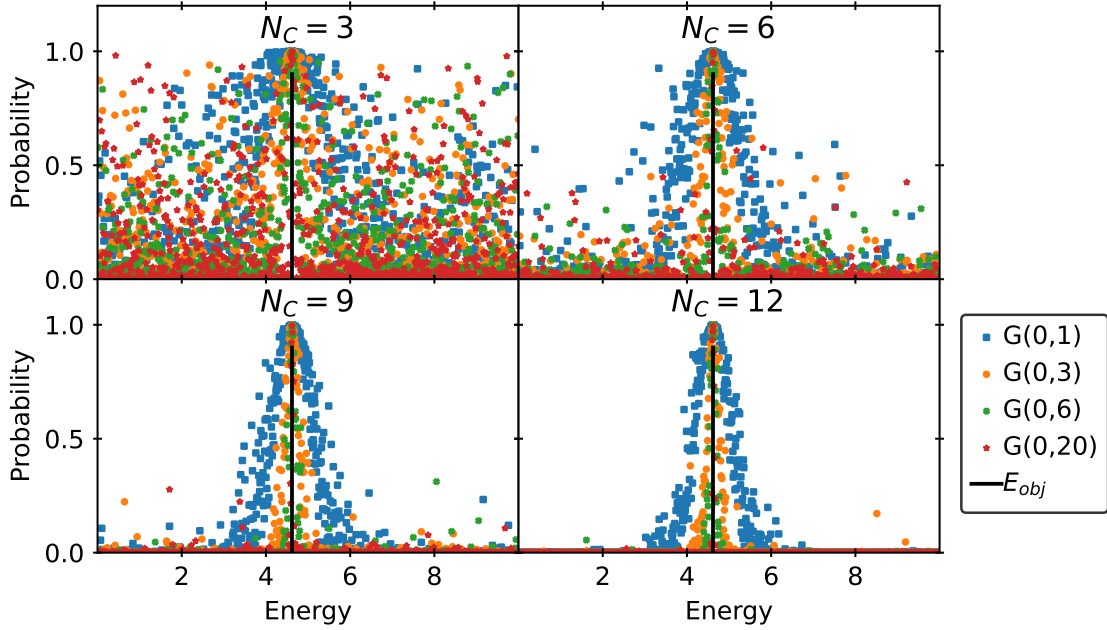
Figure 2.8: Same as Fig. (2.7) but for $N_C = 3,6,9,12$ and the reference state $|\psi_I\rangle = |E_{obj1}\rangle$. The probabilities are given with color circles instead the lines in Fig. (2.7) because we are representing rodeo probability using unaveraged random times from Eq. (2.21), instead of the analytical expression corresponding to the average of the Gaussian distribution from Eq (2.22).

figure demonstrates that the obtained spectra exhibit dispersion or noise, which can make it challenging to resolve the individual peaks, especially when a smaller number of cycles, such as $N_C = 3$, is considered.

Increasing the number of cycles, N_C, proves beneficial to mitigate the effects of noise and improve peak resolution. As shown in Fig. (2.8), the noise diminishes and the peaks become more distinct as N_C increases. This noise reduction occurs irrespective of the standard deviation of the Gaussian distribution for the random times.

Additionally, Fig. (2.8) emphasizes that the width of the peak decreases when both the standard deviation of the random Gaussian times distribution and the number of rodeo cycles, N_C, are increased. This reduction in width indicates improved resolution and precision in identifying the eigenenergies.

To mitigate the noise and enhance the accuracy of the probability estimates, an alternative approach is to repeat the rodeo algorithm multiple times with different sets of random times, and then average the resulting probabilities. By performing this averaging procedure with a sufficiently large number of repetitions, we can expect to recover the probability distributions depicted in Fig. (2.5) and (2.6), as derived analytically. Averaging the rodeo probability N_{av} times yields the following expression for the probability, represented as P_{N_C},

$$(P_{N_C})_{t_n \to G(0,\sigma_t)} = \frac{\sum_n^{N_{av}} \prod_n^{N_C} \sum_i c_i^2 \left[\cos^2 \left(\frac{t_n(E_{obj\,i} - E)}{2} \right) \right]_{t_n \to G(0,\sigma_t)}}{N_{av}}. \qquad (2.23)$$

Fig. (2.9) visualizes this approach, showing the probability distributions obtained from averaging the rodeo probability over N_{av} repetitions. In this Figure, we take
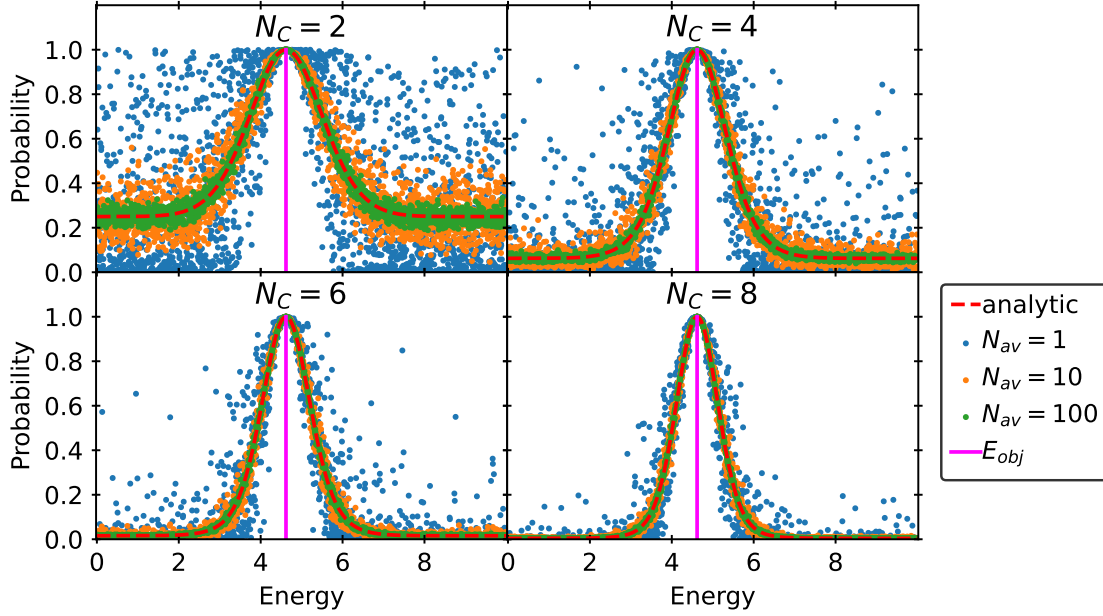
Figure 2.9: Same as Fig. (2.8) for a reference state $|\psi_I\rangle = |E_{obj1}\rangle$ and $N_C = 2,4,6,8$ and Gaussian distribution centered in $\mu = 0$ and standard deviation $\sigma_t = 1$. The probabilities are result of no averaging (blue), averaging 10 times (orange), averaging 100 times (green), and the analytically average probability in the dashed red line.

as the reference state $|\psi_I\rangle = |E_{obj1}\rangle$ as we want to observe only one peak in order to better observe the effects, and we show the probability taken different values for the rodeo cycle. As the number of repetitions increases, the probability distribution converges to the analytical expression Eq. (2.21) that was initially expected.

To calculate the parameters that define the peaks observed in the previous figures, where we consider the probability of the rodeo algorithm using random times following a Gaussian distribution, Eq. (2.21), we can leverage the analytical function since it corresponds to the average probability. Using the analytically averaged functions with random Gaussian times centered at 0, we can estimate the baseline value, bl, which represents the probability that the rodeo algorithm tends to converge to for energies far from the eigenenergies. Additionally, we can determine the width of the peak as a function of the number of rodeo cycles, N_C, and the standard deviation σ_t of the Gaussian times distribution.

For simplicity, we use one of the eigenvectors as a reference state to have only one peak in the spectrum. To estimate the peak width, we make an approximation by fitting the analytical function for random times with a Gaussian distribution centered at $\mu = 0$ to a Gaussian function. Assuming only one peak we approximate

$$
\begin{aligned}
(P_{N_C})_{G(\sigma,0)} &= \frac{1}{2^N} \left[1 + \exp\left(-\frac{\sigma_t^2}{2}(E_{obj} - E)^2 \right) \right]^{N_C} \\
&\simeq bl + a \cdot \exp\left(-\frac{(E_{obj} - E)^2}{2\sigma^2} \right).
\end{aligned}
\tag{2.24}
$$

In this way, we estimate the parameter σ which represents the width of the peak of the probability distribution. We have made the approximation that the sum of a constant and a Gaussian function raised to the power of the number of cycles can
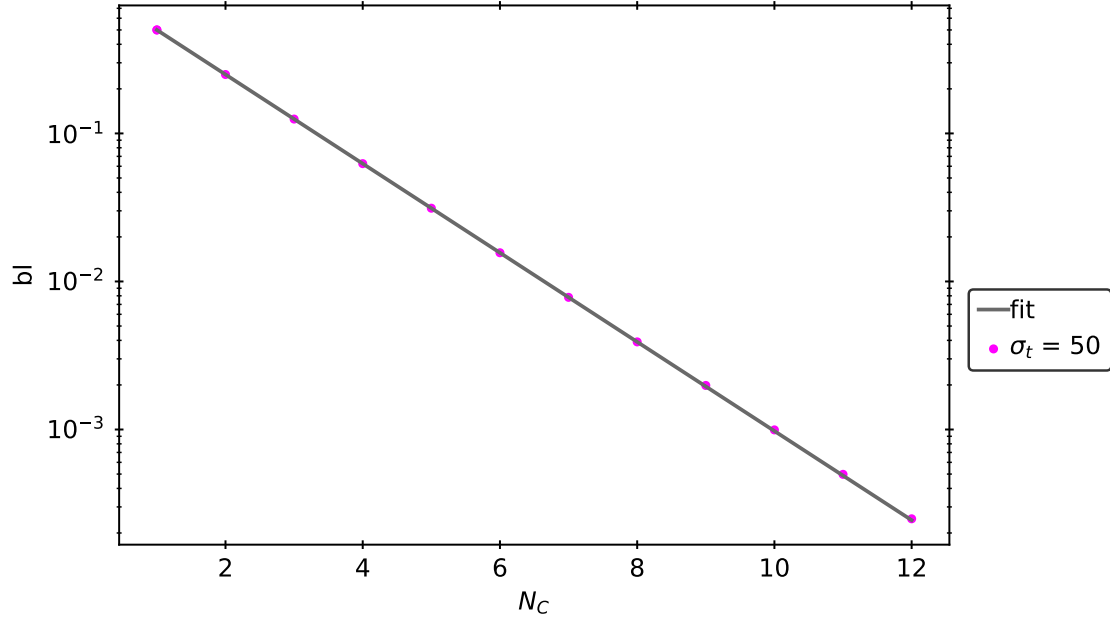
Figure 2.10: Baseline probability, bl, estimate as a function of the number of cycles, N_C, taking the reference state $|\psi_I\rangle = |E_{obj1}\rangle$ for the Hamiltonian of Eq. (2.11). The average rodeo probability is obtained using random times with a Gaussian distribution centered in $\mu = 0$ with $\sigma_t = 50$. The solid line represents the fit to the function $bl = \frac{1}{b^{N_C}}$.

be approximated by the sum of a constant, bl, and a Gaussian function with height a. This approximation allows us to simplify the analytical expression and obtain a more manageable form for further analysis and interpretation.

The fitting function Eq. (2.24) also provides an estimation of the baseline probability, which corresponds to the probability far away from the peak. In Fig. (2.10), we illustrate the estimated baseline for different numbers of rodeo cycles, N_C, and various values of σ_t, representing the standard deviation of the random times sampled from a Gaussian distribution centered at $\mu = 0$. Fig. (2.10) considers the rodeo probability for energy values far away from the eigenenergy considered.

Remarkably, the baseline estimation does not depend on the value of σ_t but solely on the number of cycles, N_C. We estimate the baseline for different values of N_C ranging from 1 to 12 and fit the data to the function:

$$bl = \frac{1}{b^{N_C}}, \tag{2.25}$$

As shown in Fig. (2.10), we obtain a very good fit, which gives the estimate

$$b = 1.99998 \pm 0.00003. \tag{2.26}$$

This value is very close to the theoretical expression Eq. (2.25), where $b = 2$,

$$bl = \frac{1}{2^{N_C}}. \tag{2.27}$$

The close agreement between the fitted value and the theoretical expectation reinforces the validity of the analytical framework. Considering the theoretical basis
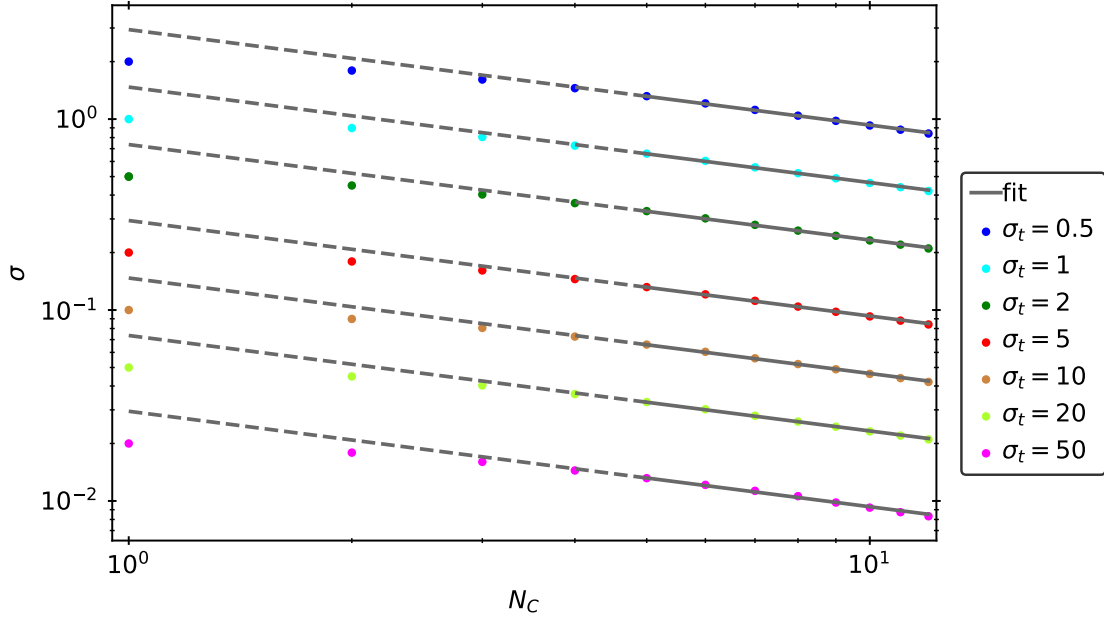
Figure 2.11: Width, σ, as a function of N_C obtained fitting Eq. (2.29) to the simulation of the rodeo algorithm at fixed σ_t. We take the reference state $|\psi_I\rangle = |E_{obj1}\rangle$ for the Hamiltonian of Eq. (2.11). Each color corresponds to a different σ_t value used for random times. Solid line correspond to the fits $\sigma = \widetilde{\sigma}_{N_C}\frac{1}{\sqrt{N_C}}$.

we have developed, we find that for N_C cycles of the rodeo algorithm, the average probability of obtaining energies far from any eigenvalues can be approximated as:

$$bl = \lim_{|E|\gg|E_{obj}|} \frac{1}{2^{N_C}} \left[1 + \exp\left(-\frac{\sigma_t^2}{2}(E_{obj} - E)^2 \right) \right]^{N_C} \rightarrow \frac{1}{2^{N_C}}, \qquad (2.28)$$

where the limit of the exponential term vanishes because its argument becomes very large and negative. This expression is in good agreement with the results obtained from the fitting of the simulation data, confirming the consistency between the theoretical analysis and the results of the rodeo algorithm simulation.

Knowing the value of the baseline, $bl = \frac{1}{2^{N_C}}$, and since the maximum probability of the peak for a state corresponding to an eigenvector is 1, we can rewrite Eq. (2.24) into the following fit function:

$$\begin{aligned}
(P_{N_C})_{G(\sigma_t,0)} &\simeq a \cdot \exp\left(-\frac{(E_{obj} - E)^2}{2\sigma_t^2} \right) + bl \\
&= \left(1 - \frac{1}{2^{N_C}} \right) \exp\left(-\frac{(E_{obj} - E)^2}{2\sigma^2} \right) + \frac{1}{2^{N_C}}.
\end{aligned} \qquad (2.29)$$

For the general case where the reference state is not an eigenvector, and c^2 can be any probability, between 0 and 1, the expression to be approximated by a Gaussian function would be

$$(P_{N_C})_{G(\sigma_t,0)} \simeq c^2 \left(1 - \frac{1}{2^{N_C}} \right) \exp\left(-\frac{(E_{obj} - E)^2}{2\sigma^2} \right) + \frac{1}{2^{N_C}}. \qquad (2.30)$$
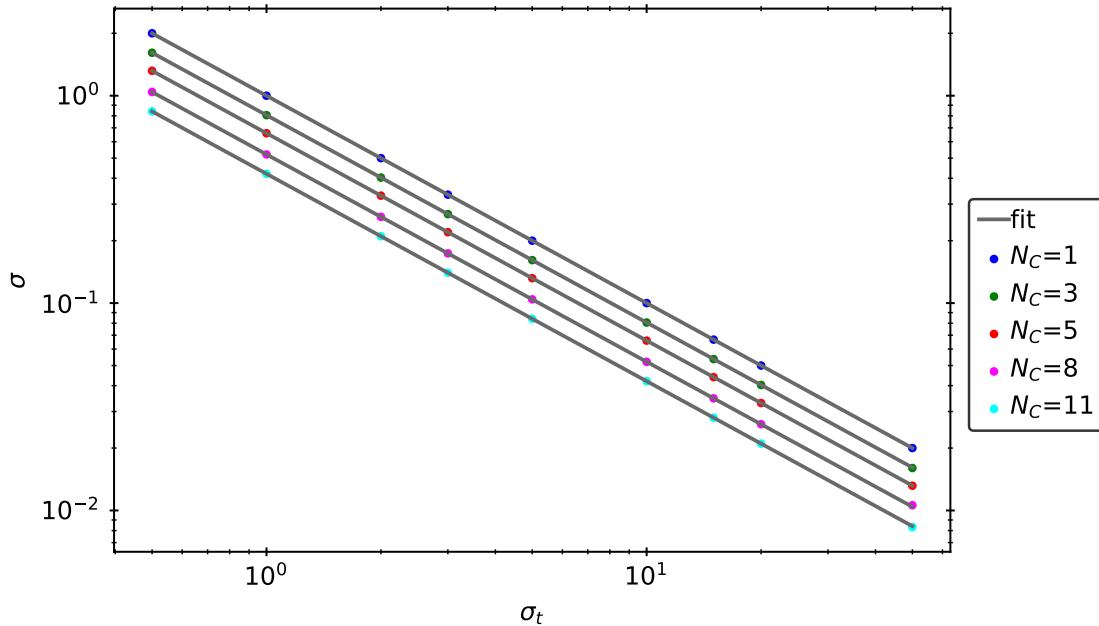
Figure 2.12: Width, σ, as a function of N_C obtained fitting Eq. (2.29) to the simulation of the rodeo algorithm at fixed σ_t. We take the reference state $|\psi_I\rangle = |E_{obj1}\rangle$ for the Hamiltonian of Eq. (2.11). Each color corresponds to a different N_C used in rodeo circuit. Solid line correspond to the fits $\sigma = \widetilde{\sigma}_{\sigma_t} \frac{1}{\sigma_t}$.

According to Ref. [11], the width of each peak that we see in the Figures where we represent the rodeo probability concerning energies is

$$\sigma = \widetilde{\sigma} \frac{1}{\sigma_t \sqrt{N_C}}, \tag{2.31}$$

where $\widetilde{\sigma}$ is a constant. In the following, we test this relationship and find the proportional parameter, $\widetilde{\sigma}$.

First, we take the parameter σ_t constant and we fit the width, σ to the function

$$\sigma = \widetilde{\sigma}_{N_C} \frac{1}{\sqrt{N_C}}. \tag{2.32}$$

for a different number of cycles. In Fig. (2.11) we show the fit for different values of σ_t. We adjust for $N_C > 4$, since $N_C \leq 3$, as we can see in the Figure, the behavior deviates from the expected relation, indicated with a dashed line. However, from 5 to 12 cycles, and $0.5 < \sigma_t < 50$, corresponding to the parameters we have taken for the fit, the behaviours fits well to the expression in Eq. (2.32).

Then, we study the dependence of the width, σ, with the standard deviation, σ_t. We keep the number of cycles N_C constant and we fit the width of the peak to

$$\sigma = \widetilde{\sigma}_{\sigma_t} \frac{1}{\sigma_t}, \tag{2.33}$$

for different values of N_C. Fig (2.12) shows that this expression fits very well the results for the parameters considered, from $1 < N_C < 11$, and from $0.5 < \sigma_t < 50$.

To determine the constant of proportionality, $\widetilde{\sigma}$, we multiply the respective constant of proportionality, $\widetilde{\sigma}_{N_C}$ and $\widetilde{\sigma}_{\sigma_t}$, by appropriate factors. In the first case, we

multiply $\widetilde{\sigma}_{N_C}$ by $\sqrt{\sigma_t}$, and in the second case, we multiply $\widetilde{\sigma}_{\sigma_t}$ by N_C. For the first case, we obtain the values listed in Table 2.1, providing an average value for the proportionality constant of 1.472 ± 0.007. The error is determined as the maximum value among the error in all the data points and the average. For the second case, we observe a slight deviation from the expected behavior for $N_C < 4$, as seen in Fig. (2.12). Therefore, we exclude these values when calculating the average. The results are presented in Table 2.2, yielding an average value of 1.48 ± 0.01 for the constant of proportionality.

Considering both sets of values, we take the average of $\langle \widetilde{\sigma} \rangle = 1.48 \pm 0.02$, where the error is the sum of the individual errors. Consequently, we can express the deviation corresponding to the width of each peak as

$$\sigma = 1.48 \cdot \frac{1}{\sigma_t \sqrt{N_C}}. \tag{2.34}$$

Table 2.1: Values of $\widetilde{\sigma}_{N_C} \cdot \sqrt{\sigma_t}$ estimated with the fits in Fig. (2.11).

σ_t	$\widetilde{\sigma}_{N_C} \cdot \sqrt{\sigma_t}$	$\delta(\widetilde{\sigma}_{N_C} \cdot \sqrt{\sigma_t})$
0.5	1.471	0.003
1	1.471	0.003
2	1.471	0.003
5	1.471	0.003
10	1.471	0.003
20	1.471	0.003
50	1.475	0.007

Table 2.2: Values of $\widetilde{\sigma}_{\sigma_t} \cdot N_C$ estimated with the fits in Fig. (2.12).

N_C	$\widetilde{\sigma}_{\sigma_t} \cdot N_C$	$\delta(\widetilde{\sigma}_{\sigma_t} \cdot N_C)$
1	1.478	0.001
3	1.455	0.001
5	1.469	0.001
8	1.474	0.001
11	1.55	0.01

2.2.3 Optimization of the rodeo circuit

In a real quantum computation, selecting appropriate parameters and design features is crucial to achieve efficient calculations and obtain the desired resolution. In this section, we estimate the minimum requirements necessary to ensure the desired results, specifically focusing on energy resolution and the minimum probability associated with each peak.

Energy interval, baseline probability and peak description

The first parameter we have to fix is the energy interval we want to examine. Our goal is to search the eigenvalues of a Hamiltonian matrix, eigenenergies. Knowing the matrix elements of the Hamiltonian matrix, we can employ the Gershgorin circle theorem [12]. This theorem gives us an energy interval for the eigenvalues:

$$\begin{aligned} \lambda_i &\leq a_{ii} + R_i, \\ \lambda_i &\geq a_{ii} - R_i, \end{aligned} \tag{2.35}$$

with the assumption the Hamiltonian is real. Here, λ_i are the eigenvalues,

$$R_i = \sum_{j \neq i} |a_{ij}|, \tag{2.36}$$

and a_{ij} are the elements of the Hamiltonian matrix, where the sub-index i, j run through all the rows and columns. Therefore, we take the minimum, $\min(a_{ii} - R_i)$, and maximum, $\max(a_{ii} + R_i)$, values to choose the interval energy to ensure that the energy range is sufficiently wide to capture all eigenvalues.

The other parameters we have to optimize are the number of cycles, N_C, the standard deviation of the Gaussian distribution of random times, σ_t, the number of energies E, N_E, where we evaluate the probability, and the number of times we do the N_C cycles for the same energy and we average over them, N_{av}.

First, we can use N_C to fix the baseline probability we want to achieve, considering that it only depends on this parameter. The baseline has to be sufficiently low to distinguish the peaks, so it has to be smaller than the maximum probability (c_i^2) of the peaks we want to evaluate, but not much more to avoid using much computing time. Fixed N_C, we can fix the number of energies, N_E, required to ensure sufficient peak width. It is crucial to have enough data points within each peak to accurately distinguish and characterize them. We can take as a parameter the number of minimum points required in the peak area, N_p. Considering the expression, Eq. (2.34), assuming a Gaussian peak width of 4σ, where σ is the standard deviation of the Gaussian distribution, we can establish the following condition, being Δ_E the interval energy between two energies,

$$N_p \Delta_E \geq \frac{4 \cdot 1.48}{\sqrt{N_C}\, \sigma_t}. \tag{2.37}$$

We can rewrite the expression in terms of the total number of energy values, N_E, and the total interval energy, $\max(a_{ii} + R_i) - \min(a_{ii} - R_i)$, being

$$\Delta_E = \frac{\max(a_{ii} + R_i) - \min(a_{ii} - R_i)}{N_E + 1}. \tag{2.38}$$

With Eqs. (2.37) and (2.38) we can rewrite the minimum energies, N_E necessary in the total interval energy:

$$N_E = \frac{(\max(a_{ii} + R_i) - \min(a_{ii} - R_i)) \cdot N_P \cdot \sqrt{N_C} \cdot \sigma_t}{4 \cdot 1.48} + 1. \tag{2.39}$$

Indeed, as indicated in Eq. (2.39), the number of minimum energies required increases with the number of rodeo cycles and the standard deviation of the random times. This is because, as N_C and σ_t increase, the width of the peaks in the probability distribution decreases, resulting in a higher density of energy points needed to adequately sample each peak.
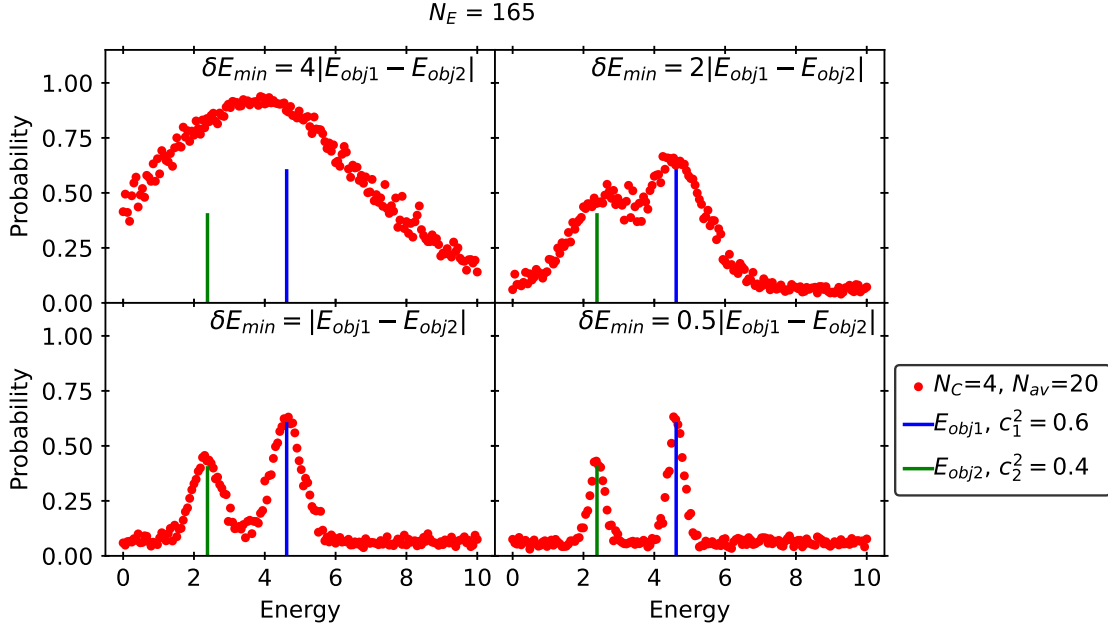
Figure 2.13: Rodeo probability for $N_C = 4$ cycles for different values of energy (in A.U.) taking the state $|\psi_I\rangle = \sqrt{0.6}|E_{obj1}\rangle + \sqrt{0.4}|E_{obj2}\rangle$ for the Hamiltonian of Eq. (2.11). Using random times with Gaussian distribution centered in $\mu = 0$ and different standard deviations obtained from Eq. (2.41) so that the minimum energy difference between two resolvable peaks is: $\delta E_{min} = 4, 2, 1$, and 0.5 times the magnitude $|E_{obj1} - E_{obj2}|$, that corresponds to $\sigma_t = 11.18, 4.47, 2.24, 1.12$. The probability has been averaged 20 times, $N_{av} = 20$ for each energy taken in the rodeo cycle.

Energy resolution of rodeo algorithm

To determine the value of the parameter σ_t in the rodeo algorithm, we need to consider the minimum difference (δE_{min}) between two eigenvalues that we want to distinguish. Considering that two peaks resolvable when we can see 4σ of their width without overlap with another peak, the minimum value of σ_t, considering the estimation Eq. (2.34), is

$$\sigma_t = \frac{4 \cdot 1.48}{\sqrt{N_C}\,\delta E_{min}}. \tag{2.40}$$

The minimum value of σ_t value increases when aiming for a higher resolution, as narrower peaks are required to achieve better distinguishability. Considering this σ_t, the minimum points necessary by the rodeo algorithm corresponds to:

$$N_E = \frac{(\max(a_{ii} + R_i) - \min(a_{ii} - R_i)) \cdot N_P}{\delta E_{min}} + 1. \tag{2.41}$$

So it depends mainly on the resolution required between the eigenenergies and the number of energies we consider adequate to be able to detect a peak due to an eigenenergy.

In Fig. (2.13), we present the rodeo probability for the reference state $|\psi_I\rangle = \sqrt{0.6}|E_{obj1}\rangle + \sqrt{0.4}|E_{obj2}\rangle$ using different values of σ_t. We choose these values of σ_t based on the minimum energy resolution required, δE_{min}, which we set to 4, 2, 1,

and 0.5 times the magnitude of $|E_{obj1} - E_{obj2}|$, as determined by Eq. (2.40). The Figure demonstrates how the two peaks are resolved for different standard deviations in the random times. We observe three scenarios: when δE_{min} is greater than the energy difference between the two eigenvalues $|E_{obj1} - E_{obj2}|$, When is equal and when it is lower. For $\delta E_{min} = 4|E_{obj1} - E_{obj2}|$ the two peaks cannot be distinguished and are seen as a single peak. When $\delta E_{min} = 2|E_{obj1} - E_{obj2}|$, the two peaks are partially resolved, but they still overlap significantly. When $\delta E_{min} = |E_{obj1} - E_{obj2}|$ the two peaks are practically resolved as we can distinguish them. Finally, when $\delta E_{min} = 0.5|E_{obj1} - E_{obj2}|$, the two peaks are well-separated and completely resolved.

In Fig. (2.13), it is evident that the height of the peak in the rodeo probability distribution depends on the value of σ_t. When the two peaks are not resolvable and σ_t is relatively small, we observe a single peak that corresponds to the superposition of two eigenenergies. As σ_t decreases, the peak becomes broader and taller, approaching the combined height of the individual peaks representing each eigenvalue. Moreover, the center of the peak tends to align more closely with the eigenvalue that has a higher probability of c_i^2.

Overall, the results obtained from the analysis align with our expectations based on the estimated expression, Eq. (2.40). The minimum deviation in σ_t enables the resolution of two eigenvalues with a minimum energy difference of δE_{min}. This demonstrates the effectiveness of the rodeo algorithm in distinguishing closely spaced eigenenergies and supports its potential for solving quantum systems with high precision.

Uncertainty in rodeo algorithm

In section 2.2.1, we have optimized the different parameters by considering the rodeo probability as the analytical average over the times with a Gaussian distribution centered at $\mu = 0$, Eq. (2.21). Next, we will study how the noise caused by the random times is affected by considering Eq. (2.22). We study the uncertainty in terms of the different parameters of interest by means of the number of rodeo cycles, N_C and the number of times we average, N_{av}, since as we have seen in chapter 2 these are the two parameters that decrease the noise caused by the random numbers. We focus on estimating the uncertainty in the parameters E_{obj} and c_i^2 since these are the values we aim to determine using the rodeo algorithm. We also estimate the uncertainty in the baseline, as it can help us optimize the value of N_C. To assess the impact of noise, we will consider 10 energy values within each peak ($N_P = 10$).

For simplicity, we take as reference state the eigenvector $|E_{obj1}\rangle$ to deal with only one peak. We fit the following expression

$$(P_{N_C})_{\rho \to G(0,\sigma_t)} = c^2 \frac{1}{2^{N_C}} \left[1 + \exp\left(-\frac{\sigma_t^2}{2}(E_{obj} - E)^2 \right) \right]^{N_C}, \qquad (2.42)$$

as we want to fit the parameters c_i^2 and E_{obj} with the objective to know the accuracy with which we can obtain them with the rodeo algorithm. We take as the error the standard deviation, the square root of the variance of the fit itself. As the value of the standard deviation for the random times following a Gaussian distribution centered at $\mu = 0$, we choose $\sigma_t = 1$, which let us see the peak properly.

In Fig.(2.14) shows the uncertainty obtained for c_i^2 from the given in Eq.(2.42). Since the values of δc_i^2 consistently align with the expected value of 1 within their
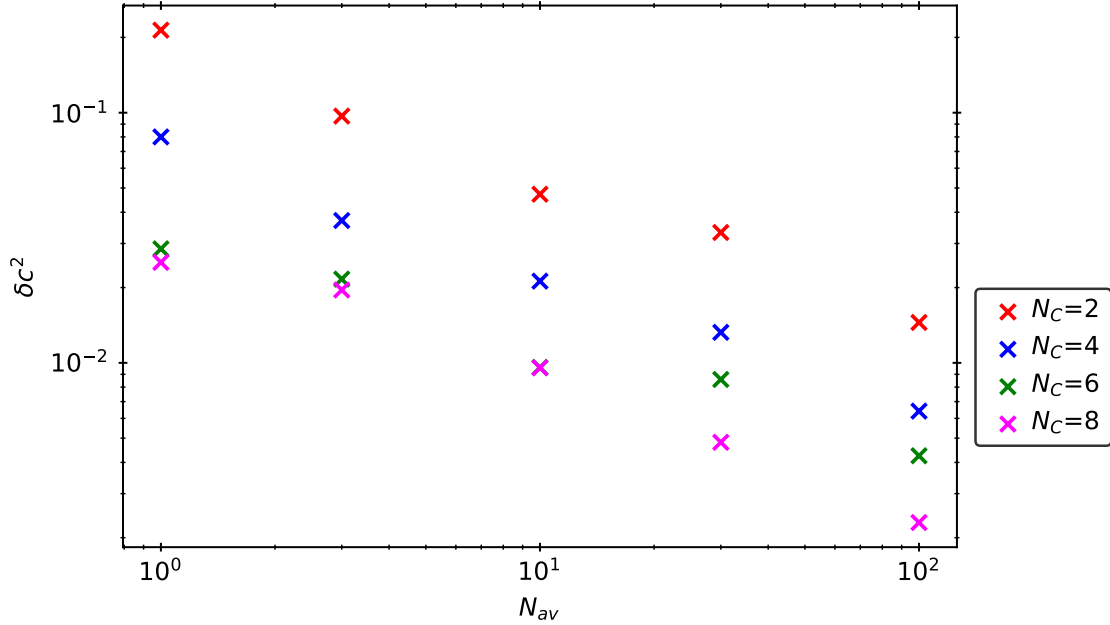
Figure 2.14: Uncertainty of the estimated parameter c^2, as a function of the number of averages used in the rodeo probability, N_{av}, for different values of N_C represented with different colors. We use the reference state, $|\psi_I\rangle = |E_{obj1}\rangle$ and the number of energies values has been taken so that there are 10 energies values, $N_P = 10$ within the peak.

associated errors, we exclude them from further analysis. The double logarithmic plot in Fig.(2.14) shows an approximately linear relationship, allowing us to estimate the logarithms of δc_i^2 and the number of averages as a straight line for each value of N_C cycles. We fit the error of c^2 for each considered N_C to the expression

$$\delta c^2 = a_1 \cdot N_{av}{}^{b_1}, \tag{2.43}$$

where a_1 and b_1 are constants. Considering the stochastic nature of random numbers, we perform this calculation ten times, using different random times for each iteration, and average the values of a_1 and b_1 as presented in Table (2.3). In each case, we choose the decimal places according to the error of each value.

We consider a unified expression that takes into account the results for each of

Table 2.3: Average values for δc_i^2, found by fitting to the results obtained with the rodeo algorithm to the expression in Eq. (2.43) ten differents times for different number of cycles N_C.

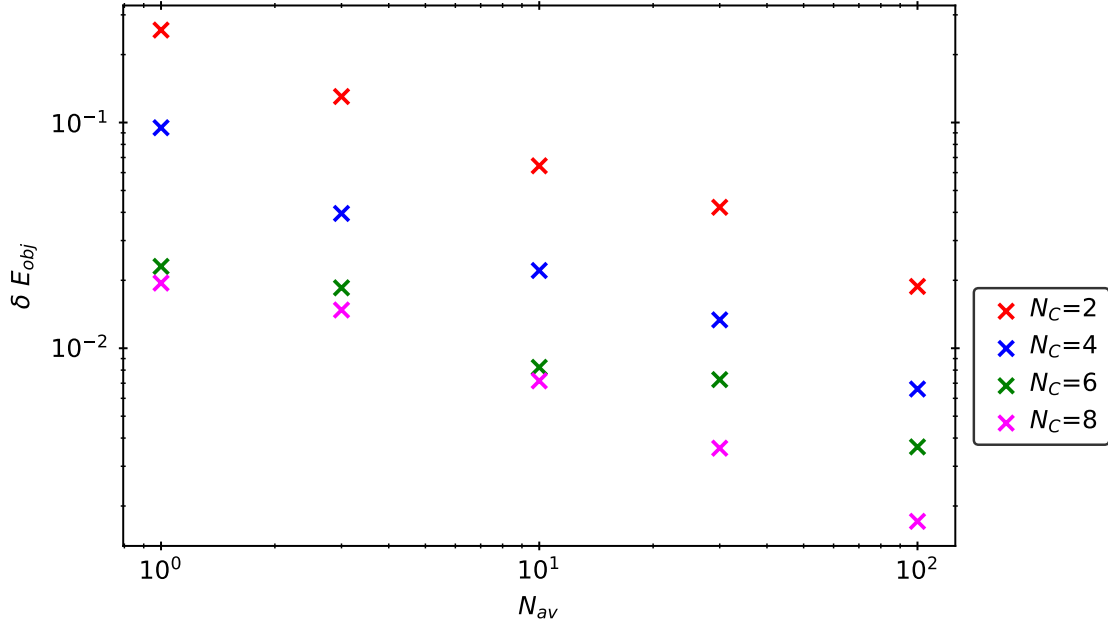| N_C	$\widetilde{a_1}$	$\widetilde{b_1}$
2	0.16	-0.52
4	0.08	-0.54
6	0.043	-0.51
8	0.024	-0.53

Figure 2.15: Same as Fig. (2.14) but for the uncertainty eigenenergy δE_{obj} case.

the considered rodeo cycles. As for the exponent of the number of averages $\widetilde{b}_1$ in the rodeo cycle, we see in Table (2.3) that remains approximately constant with N_C. Therefore, we take the mean value of $\widetilde{b}_1$. For the proportional value, $\widetilde{a}_1$, we observe a linear relationship on the double logarithmic scale with respect to the number of cycles, N_C. To capture this dependence, we fit the parameters to the expression

$$a_1 = a_2 \cdot N_C^{b_2}, \tag{2.44}$$

yielding a result of a best fit

$$a_1 = 0.40 \cdot N_C^{-1.2}. \tag{2.45}$$

Based on these observations, we approximate the uncertainty of c_i^2 as follows:

$$\delta c^2 \simeq 0.40 N_C^{-1.2} N_{av}^{-0.53}. \tag{2.46}$$

We do the same analysis for the case of the eigenenergy uncertainty, δE_{obj}, from the peak we have considered since we see that the behavior of the error in the eigenenergy is very similar to that of c^2. Fig. (2.15) shows the uncertainty for E_{obj} from a fit of the results of the rodeo algorithm to the expression in Eq. (2.42). In turn, We fit the uncertainty to the expression

$$\delta E_{obj} = a_3 \cdot N_{av}^{b_3}, \tag{2.47}$$

and we obtain the average values in Table 2.4, averaging also ten times as c^2.

Given the similarity observed in the behavior of c_i^2, we follow the same procedure of unifying the expressions for each value of N_C. After analyzing the results, we arrive at the following unified expression:

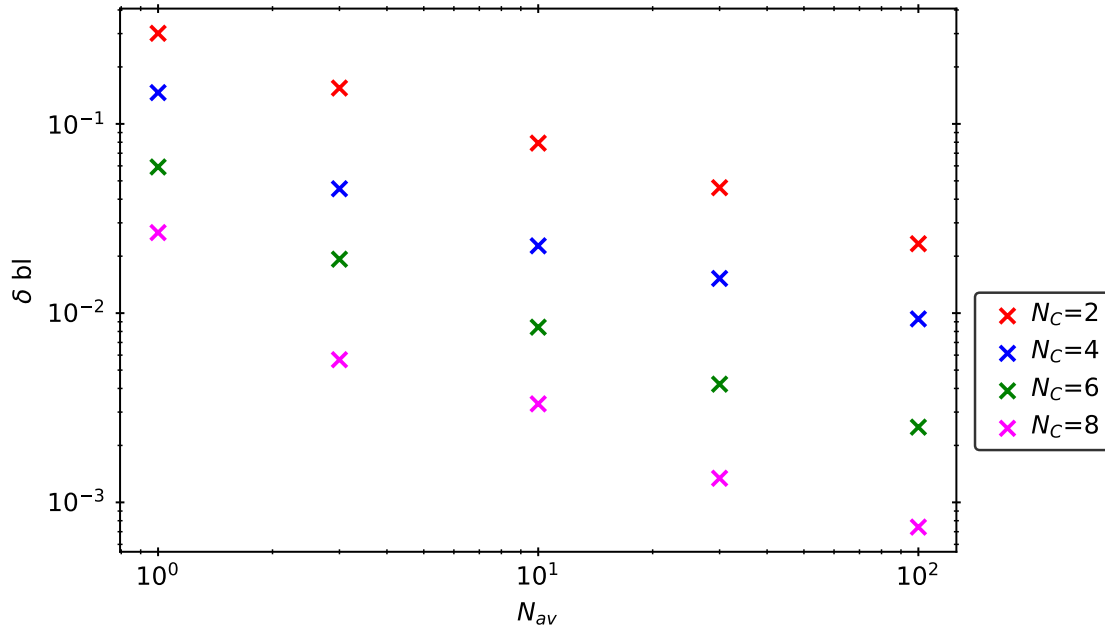$$\delta E_{obj} \simeq 0.49 N_C^{-1.3} N_{av}^{-0.52}. \tag{2.48}$$

Figure 2.16: Same as Fig. (2.14) but for the uncertainty of the baseline probability δbl.

For the calculation of the uncertainty of the baseline probability, we consider the average of 40 values of the rodeo probability for energy values that are sufficiently far from the peak. By averaging multiple values, we can reduce the impact of fluctuations and obtain a more reliable estimation of the baseline probability.

We do the same analysis for the case of the baseline uncertainty, δbl, as in the two previous cases. In Fig. (2.15) we plot the uncertainty values obtained for bl and fit them using Eq.(2.42). We fit the uncertainty, for each N_C, to the expression

$$\delta bl = a_4 \cdot N_{av}{}^{b_4}, \tag{2.49}$$

representing the average values in Table 2.5.

Given the similarity observed in the behavior of the two previous cases, we follow the same procedure of unifying the expressions for each value of N_C. We fit this time the average values $\widetilde{a_4}$ considering their behavior, for the different N_C to the

Table 2.4: Average values for δE_{obj}, found by fitting to the results obtained with the rodeo algorithm to the expression in Eq. (2.47) ten differents times for different number of cycles N_C.

N_C	$\widetilde{a_3}$	$\widetilde{b_3}$
2	0.20	-0.52
4	0.08	-0.53
6	0.036	-0.51
8	0.024	-0.53

Table 2.5: Average values for δbl, found by fitting to the results obtained with the rodeo algorithm to the expression in Eq. (2.49) ten differents times for different number of cycles N_C.

N_C	$\widetilde{a_4}$	$\widetilde{b_4}$
2	0.28	-0.52
4	0.11	-0.52
6	0.036	-0.55
8	0.008	-0.54

expression

$$a_4 = a_5 \exp\left(b_5 \cdot N_C\right). \tag{2.50}$$

After analyzing the results, we approximate the uncertainty of bl as follows:

$$\delta bl \simeq \exp\left(-0.6 \cdot N_C\right). \tag{2.51}$$

Overall, we observe that, in all cases, the uncertainty decreases more rapidly with the number of cycles, N_C, than with the number of averages, N_{av}. This suggests that increasing the number of cycles has a more significant impact on reducing the uncertainty compared to increasing the number of averages.

Chapter 3

Rodeo algorithm for ^{6}Li

In this chapter, we implement the estimations and expressions developed in the previous chapter, this time considering a realistic Hamiltonian. First, we outline the expressions that guide our parameter selection for the rodeo circuit. Subsequently, we apply these expressions in various cases, comparing the results obtained from the rodeo algorithm with the exact solutions for the Hamiltonian by direct diagonalization. This allows us to assess the effectiveness of the rodeo algorithm in solving the specific problem at hand.

3.1   Choice of rodeo algorithm parameters

In our realistic case, we consider the ^{6}Li nucleus using the Cohen-Kurath interaction in the p shell [13]. We show the diagram of the p shell of the harmonic oscillator in Fig. (3.1). This Hamiltonian corresponds to a 10×10 matrix. Following the analysis in chapter 2, we calculate the minimum values of the rodeo algorithm parameters to find the eigenvalues of the Hamiltonian for a given resolution. To find the eigenenergies employing the rodeo algorithm, we first calculate the upper and lower bound where the eigenenergies are to be found, using the Gershgorin circle theorem, Eqs. (2.35), that they correspond to $E_{obj\,min} \simeq -10.5$ MeV, $E_{obj\,max} \simeq 14.4$ MeV.

Next, we need to determine the minimum number of rodeo cycles, N_C, required to detect peaks associated with an energy measurement of the reference state with probability c_i^2 larger than a minimum one, P_{min}. To ensure this, P_{min} must be above the baseline probability, including its uncertainty due to use of random times. Additionally, we consider the uncertainty estimated for c^2. Thus, the following
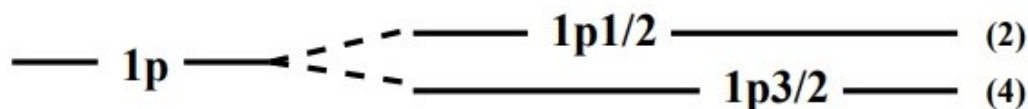

Figure 3.1: Harmonic oscillator diagram of the p shell from [14]. In the context of the shell model in nuclear physics, the notation nlj refers to the quantum numbers used to label the single-particle states or orbitals. In the p-shell, which consists of orbitals with l=1, the possible quantum numbers for the single-particle states can be denoted as p1/2 and p3/2
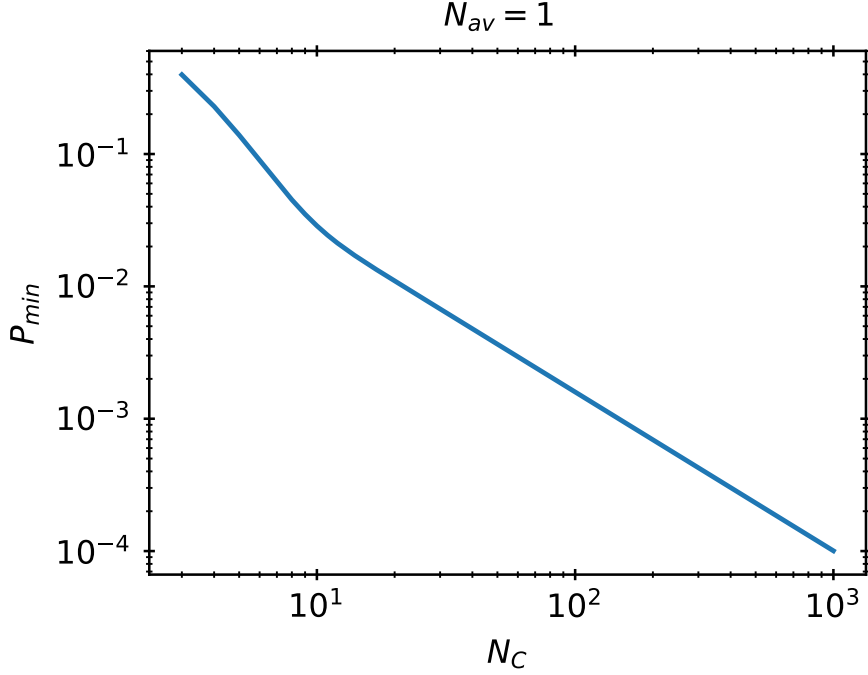
Figure 3.2: Minimum value for c_i^2, P_{min}, that we can obtain from the expression Eq. (3.1) evaluated by different values of N_C. We have considered $N_{av} = 1$.

condition must be satisfied:

$$bl + \delta bl + \delta c^2 \simeq \frac{1}{2^{N_C}} + \exp\left(-0.6 N_C\right) N_{av}^{-0.53} + 0.40 N_C^{-1.2} N_{av}^{-0.53} \leq P_{min}, \quad (3.1)$$

where we have used the expressions in Eqs. (2.27), (2.51) and (2.46). We can represent the expression Eq. (3.1) in Fig. (3.2), where we fix the number of averages used in the rodeo cycle, $N_{av} = 1$. By doing so, we can observe the minimum probabilities, P_{min}, for a given reference state $|\psi_I\rangle$, that we are able to find based on the number of cycles used in the rodeo algorithm.

In addition, we take into account the estimation in the uncertainty of the peak energies, based on the resolution, δE_{min}, that we want to have. We consider the maximum uncertainty as σ, referred to as the estimated width of the peak. Therefore we take $\delta E_{min} = 4\sigma$ for the minimum value needed to resolve two peaks that are closer to each other. Therefore, the number of minimum cycles must also fulfill:

$$\delta E_{obj} \simeq 0.49 N_C^{-1.3} N_{av}^{-0.52} \text{ MeV} \leq \frac{\delta E_{min}}{4} \text{ MeV}, \quad (3.2)$$

where we have used the expression in Eq. (2.48).

We consider that the minimum number of cycles must be at least 3, $N_{C\,min} = 3$, since for the calculation of the minimum number of points and σ_t, we have estimated the peak width using Eq. (2.34), where we have seen that the general behavior is not fulfilled for small N_C, fitting closely to one calculated from $N_C = 3$.

We estimate the σ_t, used for random Gaussian times centered in $\mu = 0$, from the expression in Eq. (2.40) using the resolution we want to achieve, δE_{min}. As for the number of energy values, we use Eq. (2.39) estimation. We consider $N_P = 10$ since after testing with different examples, we have seen that below this value, and

considering the uncertainty of the energy values, the energy values of the peak do not fit so well to the expected expression, Eq. (2.21). Thus, following Eq. (**??**) the total number of energy values where we evaluate the rodeo probability corresponds to the following expression

$$N_E = \frac{10(E_{obj\,max} - E_{obj\,min})}{\delta E_{min}} + 1. \tag{3.3}$$

To determine which points correspond to a peak in the rodeo probability distribution, we consider a criterion where at least 7 consecutive points must be above the baseline probability. This criterion is chosen to account for the effects of uncertainty caused by random times. While 10 consecutive points would correspond to the expected width of a Gaussian peak, we allow for a slightly lower number of consecutive points to be above the baseline to accommodate possible uncertainties in the estimation process due to the uncertainty caused by considering random times.

Once a peak is found, we fit it to the analytical expression corresponding to the average of the random times with a Gaussian distribution, Eq. (2.21). To fit each of the peaks separately in the range of peak energies considering that it is far enough away from the other peaks, we approximate the expression to

$$(P_{N_C})_{G(0,\sigma_t)} \simeq c_i{}^2 \frac{1}{2^{N_C}} \left[1 + \exp\left(-\frac{\sigma_t^2}{2}(E_{obj\,i} - E)^2 \right) \right]^{N_C} + \left(1 - c_i^2\right) \frac{1}{2^{N_C}}, \tag{3.4}$$

where we have taken into account that the other peaks, which are far enough far away from a given one, contribute a value of $c_{j\neq i}^2$ multiplied by the baseline probability, Eq. (2.27), and that $\sum_i c_i^2 = 1$.

First, we calculate the probabilities simulating the rodeo algorithm, and then we fit them to Eq. (3.4). Thus, we obtain the values of c_i^2 and E_{obj} along with their corresponding errors from the fit. To account for the uncertainty in the eigenenergies, we include the width of the peak, σ, in the error estimation. We estimate the width by fitting the peak to a Gaussian function, as described in Eq. (2.30).

To ensure that we are not assigning as peaks, and therefore to the system's eigenenergies, energies that do not correspond to any eigenvalue, we keep only those that satisfy $c_i^2 \geq P_{min}$. In this way, we avoid assigning peaks to possible energy values that meet the requirements that we have considered, due to randomness.

As we have seen in Fig. (2.13), two peaks can be well resolved when taking as the minimum resolution $\delta E_{min} = |E_{obj1} - E_{obj2}|$ where 1 and 2 refer to two peaks nearby, we see how they are practically resolved. However, it may be that all probabilities are above the baseline, and then the peak can be considered as a single peak. To avoid this, for each detected peak, in addition to fitting the points to the expression in Eq. (3.4) which corresponds to a single peak, we fit it to the following expression, which considers the sum of two peaks

$$(P_{N_C})_{G(0,\sigma_t)} \simeq c_1{}^2 \frac{1}{2^{N_C}} \left[1 + \exp\left(-\frac{\sigma_t^2}{2}(E_{obj\,1} - E)^2 \right) \right]^{N_C} +$$
$$c_2{}^2 \frac{1}{2^{N_C}} \left[1 + \exp\left(-\frac{\sigma_t^2}{2}(E_{obj\,1} - E)^2 \right) \right]^{N_C} + \left(1 - c_1^2 - c_2^2\right) \frac{1}{2^{N_C}}. \tag{3.5}$$

To determine whether we are dealing with two separate peaks instead of a single peak, we compare the errors obtained from fitting Eq. (3.5) with the errors obtained

Table 3.1: Values of the eigenenergies and their respective probabilities obtained by direct diagonalization for the $|\psi_I\rangle$ state considered in Eq. (3.7) in order from lowest to highest energy.

$E_{obj\,i}$ (MeV)	c_i^2
-5.557	0.0004
-3.418	0.020
-3.049	0.069
-0.492	0.029
-0.325	0.100
0.478	0.00006
3.815	0.450
4.763	0.100
4.892	0.200
8.453	0.031

from fitting the points to the expression in Eq. (3.4). If the errors in the c_i^2 value for a single peak of the two-peak fit are smaller than the error of c_i^2 obtained from the single peak fit, this indicates the presence of two distinct peaks. In addition, we impose that for each of the peaks, c_i^2, considering Eq.(3.5) must be larger than the minimum, P_{min}. In the case of considering the sum of two peaks, we approximate the width, σ for each, σ_1 and σ_2 as

$$
\begin{aligned}
(P_{N_C})_{G(\sigma_t,0)} &\simeq c_1^2 \left(1 - \frac{1}{2^{N_C}} \right) \exp\left(-\frac{(E_{obj\,1} - E)^2}{2\sigma_1^2} \right) \\
&+ c_2^2 \left(1 - \frac{1}{2^{N_C}} \right) \exp\left(-\frac{(E_{obj\,2} - E)^2}{2\sigma_2^2} \right) + \frac{1}{2^{N_C}} .
\end{aligned}
\tag{3.6}
$$

3.2 Calculation of the energy spectrum of ^{6}Li

Let us consider a reference state $|\psi_I\rangle$ such that, in the basis of the Hamiltonian, it reads

$$
|\psi_I\rangle = [\sqrt{0.1}, \sqrt{0.1}, \sqrt{0.1}, -\sqrt{0.1}, \sqrt{0.1}, \sqrt{0.1}, \sqrt{0.1}, \sqrt{0.1}, -\sqrt{0.1}, \sqrt{0.1},]. \tag{3.7}
$$

To calculate the rodeo probability for each of the energies to be considered, we use Eq.(2.9). Even though they can be calculated by direct diagonalization, in principle we do not know the eigenvalues in advance and our goal si to find them. An exact diagonalization gives us the eigenvalues along with their squared probabilities for the $|\psi_I\rangle$ state considered in Eq. (3.7). The results are listed in Table 3.1.

First, we look for the eigenenergies that ensure that their maximum probabilities are greater than or equal to 0.2, $c^2 \geq 0.2$, and that the minimum distance to resolve two eigenvalues is 0.5 MeV, $\delta E_{min} = 0.5\,MeV$. Considering that we do not want to average, $N_{av} = 1$, we see that the minimum value of rodeo cycles we need for Eq. (3.1) and (3.2) to be satisfied is $N_C = 5$. The minimum σ_t to obtain the 0.5 MeV resolution corresponds to 5.4 while the minimum number of energies where we
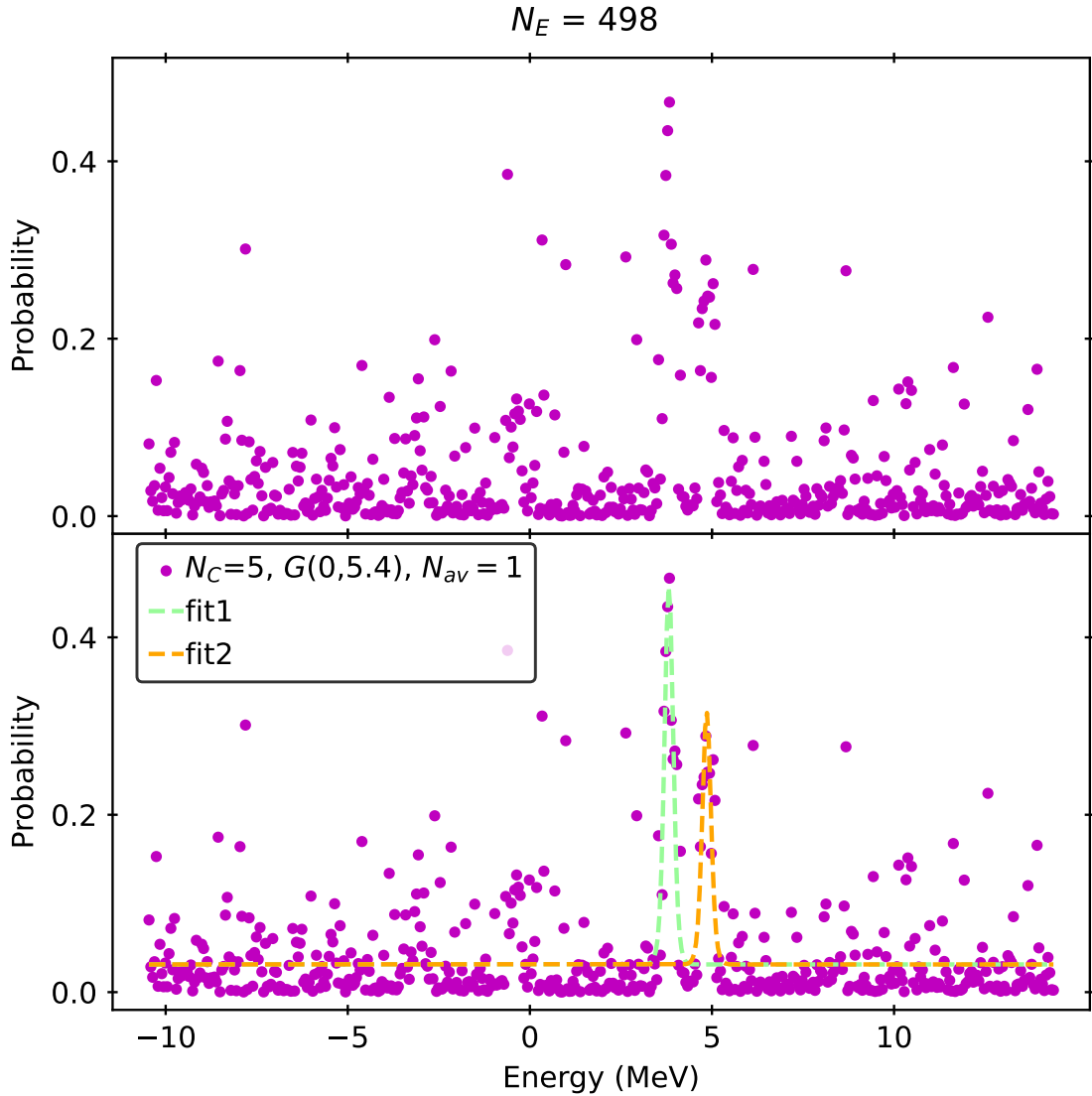
Figure 3.3: Rodeo probability for $N_C = 5$ evaluated for different energy values taking the reference state $|\psi_I\rangle$ given by Eq. (3.7) for ^{6}Li. The figure shows results using random times with Gaussian distribution centered in $\mu = 0$ and standard deviation $\sigma_t = 5.4$, without averaging the total rodeo probability for each energy and evaluating the probabilities in 498 energies. In the bottom panel, we also show the fits for the peaks found by our rodeo algorithm for a resolution $\delta E_{min} = 0.5$ MeV and $P_{min} = 0.2$ with the algorithm developed.

evaluate the rodeo probability, corresponds to $N_E = 498$ in the whole interval from $E_{obj\,min}$ to $E_{obj\,max}$, obtained from Eq. (3.3).

In Fig. (3.3), we present the probabilities obtained for each energy value using the rodeo algorithm, along with the corresponding fits for the detected peaks. As shown in the figure, our algorithm successfully detect two peaks. With our approach we do not always get the two peaks after running the rodeo algorithm, however, we do get both of them most of the times.

In Fig.(3.4), we compare the eigenenergies obtained for each peak using the fit in Eq.(3.4) with the exact diagonalization results provided in Table 3.1. Each eigenenergy is displayed with a different color, with solid lines representing eigenenergies
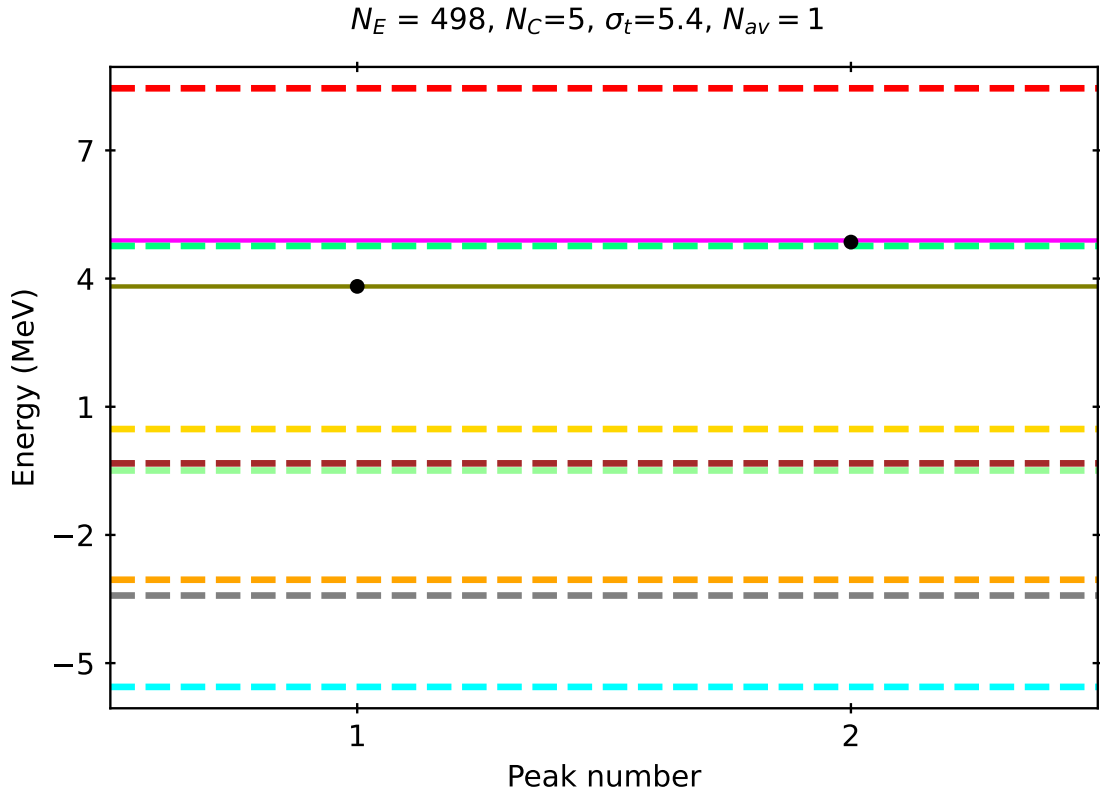
Figure 3.4: Eigenenergies obtained from the rodeo algorithm developed compared to the exact values, represented by lines of different colors, for the fits shown in Fig. (3.3). The solid lines correspond to the eigenenergies we expect to find with the rodeo algorithm given the imposed requirements, for a resolution $\delta E_{min} = 0.5$ MeV and $P_{min} = 0.2$.

satisfying $c^2 \geq 0.2$, and dashed lines representing eigenenergies with lower probabilities. We observe that the two detected peaks, shown in solid circles agree well with the exact energies.

Prior to associating each peak with its corresponding eigenvalue, we consider the value of the eigenenergy obtained from the rodeo algorithm, along with its error. If the difference between the eigenenergy obtained from the fit and the analytical value falls within the error range, we conclude that the peak corresponds to the associated eigenvalue.Figs (3.5) shows the value of c_i^2 found for each peak by fitting the results of the rodeo algorithm to Eq. (3.4) fitting compared to the exact result for the $|\psi_I\rangle$ state.

Considering the conditions imposed for P_{min} and the $|\psi_I\rangle$ state, we expect to observe a peak at an energy of $E_{obj} = 3.815$ MeV with a probability squared $c^2 = 0.450$, and another peak at $E_{obj} = 4.892$ MeV with $c^2 = 0.200$. However, it is important to note that there is an additional peak at $E_{obj} = 4.763$ MeV with $c^2 = 0.1$ (see Table 3.1). Due to the minimum resolution criterion of $\delta E_{min} = 0.5$ MeV, the second peak overlaps with this additional peak, resulting in a higher observed c^2 value.

To determine the precise association between the second peak and the corresponding eigenvalues, we compare the obtained c^2 value with those of each eigenvalue individually (represented by dashed lines) as well as their sum (represented by
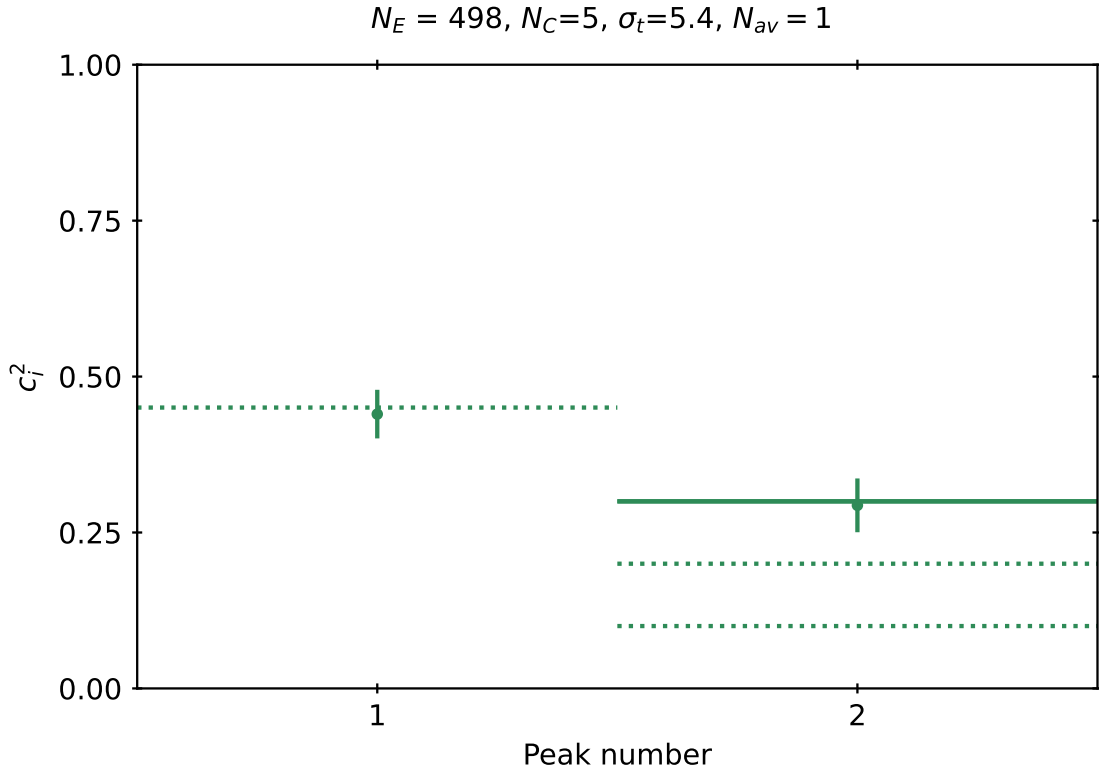
Figure 3.5: Values of c_i^2 for each peak obtained from our rodeo algorithm with the fits shown in Fig. (3.3), shown in solid errorbars, compared to the exact values. When a peak found by the rodeo algorithm coincides with multiple exact calculated eigenenergies, we represent the individual c_i^2 values with a dashed line and the sum of these values with a solid line.

a solid line). Since the obtained eigenenergy for the second peak, along with its error, matches two exact calculated eigenenergies, we expect the c^2 value to fall within the range defined by the highest c^2 value of the two eigenstates and the sum of their c^2 values. Fig. (3.5) shows that, in this case, the estimated c^2 value aligns with the sum of the individual eigenstates, supporting the conclusion that the second peak corresponds to the combined contribution of the two eigenvalues.

Doing the same analysis with the same conditions imposed, $P_{min} = 0.2$ and $\delta E_{min} = 0.5$ MeV, but averaging 10 times the rodeo probabilities for each energy, $N_{av} = 10$, according to Eq. (3.2) the minimum number of rodeo cycles corresponds to $N_C = 4$ instead of $N_C = 5$. Thus, for the standard deviation of the Gaussian random numbers centered on $\mu = 0$, the minimum value corresponds to $\sigma_t = 6$. We obtain, for this case, very similar results than using $N_{av=1}$.

As a second case of the rodeo algorithm for ^{6}Li, let us consider another case with more restrictive conditions, both for the minimum c_i^2 probability of the peaks and for the minimum resolution in the energies. With the intention of detecting more peaks with the rodeo algorithm, we consider this time $P_{min} = 0.1$ and $\delta E_{min} = 0.1$ MeV. We perform the same analysis as with the less restrictive conditions, $P_{min} = 0.2$ and $\delta E_{min} = 0.5$ MeV, without averaging the rodeo probability for each energy, N_{av}. From Eq. (3.1) and (3.2) we obtain that the minimum number of cycles corresponds to $N_C = 10$. The minimum standard deviation of the Gaussian distribution to obtain
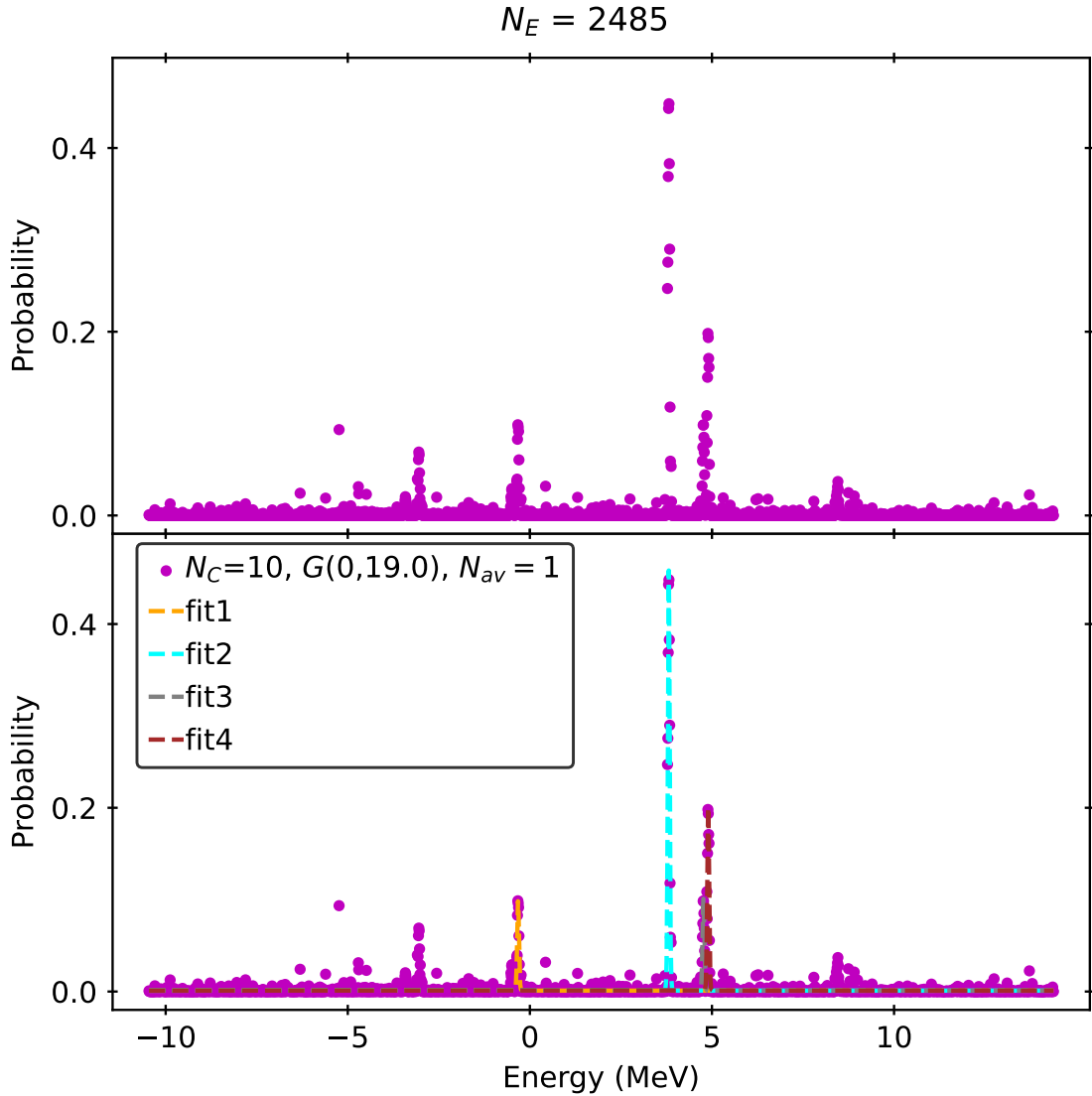
Figure 3.6: Same as Fig. (3.3) but demanding in our algorithm a resolution $\delta E_{min} = 0.1$ MeV and $P_{min} = 0.1$.

the $\delta E_{min} = 0.1$ MeV resolution corresponds to $\sigma_t = 19.0$, while the minimum energy values where we need to evaluate the rodeo probability corresponds to $N_E = 2485$, obtained from Eqs. (3.2). In Fig. (3.6), we present the probabilities obtained for each energy using the rodeo algorithm, along with the corresponding fits for the detected peaks. As shown in the figure, the algorithm successfully detect four peaks. As in the previous case, when dealing with random times, we do not always get the four peaks after running the rodeo algorithm, however, we do get it most of the time.

In Fig. (3.7) we compare the values of the eigenenergies obtained for each peak, employing the expression in Eq. (3.4) or (3.5), with the exact eigenvalues given in Table 3.1. We observe that the four peaks found have their energies very close to the expected energies, shown with solid lines. In Fig. (3.5) we show the value of c_i^2 found for each peak by Eq. (3.4) or (3.5) fitting compared to the exact results for the $|\psi_I\rangle$ state. We see how the values found agree, taking into account the error fit, with the exact results.

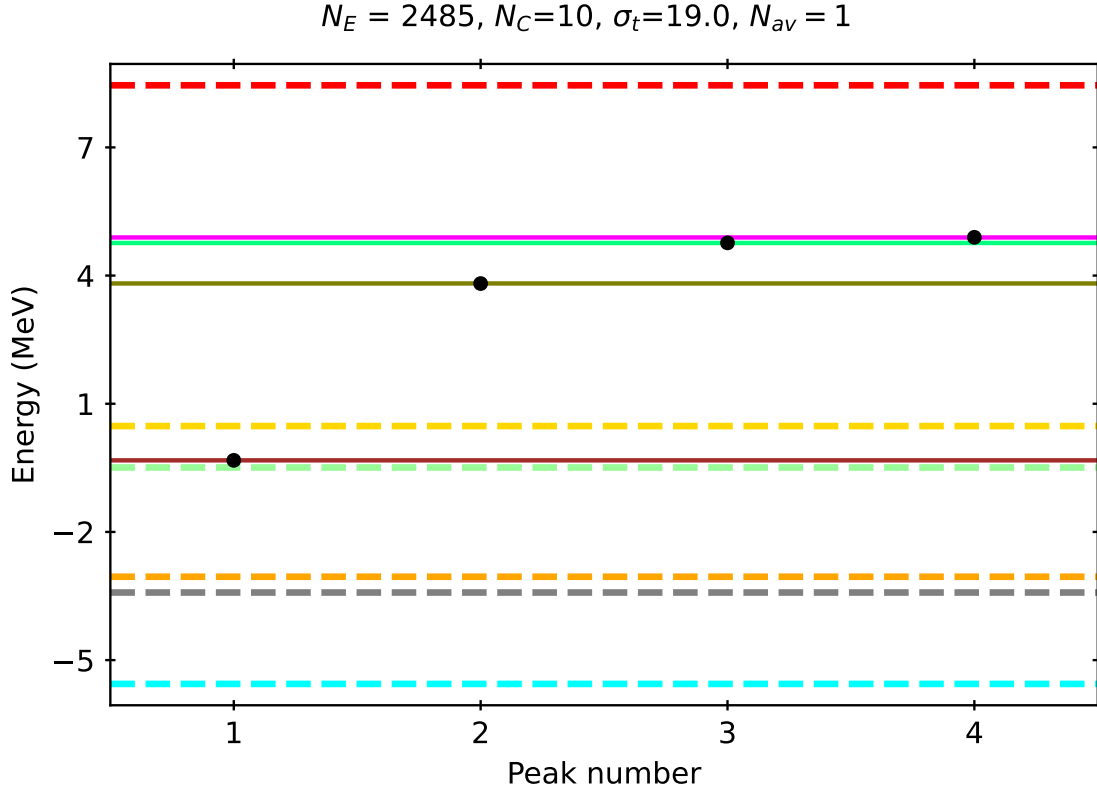Doing $P_{min} = 0.1$ and $\delta E_{min} = 0.1 MeV$, but averaging 10 times the rodeo

Figure 3.7: Same as Fig. (3.4) for the resolution $\delta E_{min} = 0.5$ MeV and $P_{min} = 0.2$ with fits shown in Fig. (3.6).

probabilities for each energy, $N_{av} = 10$, according to Eq. (3.1) and (3.2) that the minimum number of rodeo cycles corresponds to $N_C = 5$ instead of $N_C = 10$. Thus, for the standard deviation of the Gaussian random numbers centered on $\mu = 0$, the minimum value corresponds to $\sigma_t = 26.8$. We obtain, for this case, very similar results from using $N_{av} = 1$.

In order to perform an exhaustive study finding all the peaks and therefore all the eigenenergies together with their probabilities, we would need to consider a $P_{min} = 0.00006$, since it is the smallest value of c^2 as given in Table 3.1, as well as a minimum resolution of $\delta E_{min} = 0.129$ MeV. For large values of the number of cycles, N_C, Eq. (3.1) simplifies to:

$$0.40 N_C^{-1.2} N_{av}^{-0.53} \leq P_{min}, \qquad (3.8)$$

while Eq. (3.2) remains valid. Eq (3.8) has been simplified because the other terms in the expression of Eq. (3.1), decrease much more rapidly. In this manner, to find all the peaks corresponding to eigenenergies, if we do not average and take $N_{av} = 1$, we would need a minimum of $N_C = 1628$ rodeo cycles. This high value for the number of rodeo cycles is a great computational effort for the classical algorithm we have developed given our computational capacity. With the developed algorithm and our computational capacity, we can find a peak with a minimum value for the probability of $P_{min} = 0.0001$, although it corresponds to a considerable computational effort.

Based on the results obtained presented in Figs (3.4), (3.5) and (3.7), (3.8), we can conclude that the rodeo algorithm is generally successful in finding the eigenenergies of the ^{6}Li Hamiltonian and the associated probabilities of measuring these
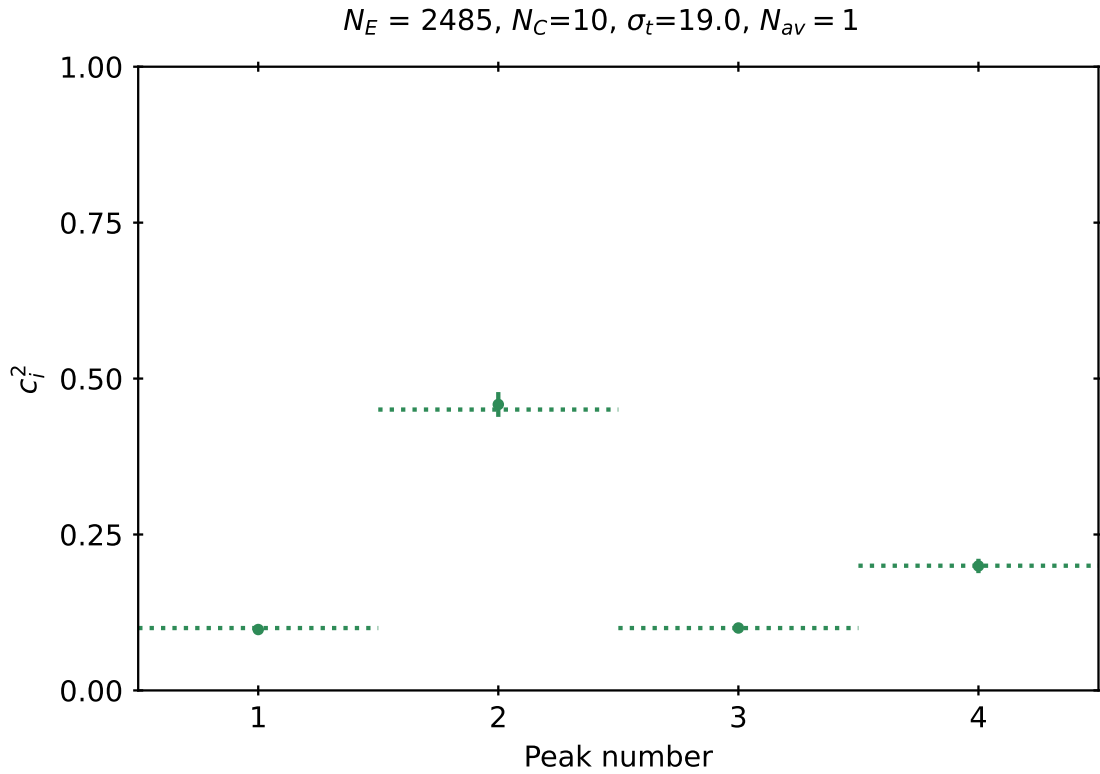
Figure 3.8: Same as Fig. (3.5) for the fits shown in Fig. (3.6).

eigenvalues for the reference state $|\psi_I\rangle$. The algorithm provides reliable and accurate results, allowing a great deal of information of the eigenstates of the system.

It is important to note that the success of the rodeo algorithm relies on appropriately choosing the parameters, such as the number of cycles N_C and the number of averages N_{av}. These parameters should be carefully selected based on the specific system and the desired level of accuracy and resolution.

Overall, the rodeo algorithm offers a valuable approach for identifying and analyzing eigenenergies and probabilities of quantum systems, providing a useful tool for quantum state analysis.

Chapter 4

Conclusions

The rodeo algorithm, implemented on a quantum computer, allows us to find the eigenenergies and probabilities for a reference state, the squared projection on each eigenvector. In order to test the capabilities of this algorithm, we have developed a classical algorithm that mimics the rodeo circuit and enables us to estimate the eigenenergies of a Hamiltonian and their corresponding squared probabilities.

In this work, we derived the expressions for the probabilities of finding the ancilla qubits in the state $|1\rangle$, within the rodeo circuit. These expressions have a time dependence for each rodeo cycle, N_C. To ensure accurate results, we introduced Gaussian random times centered at $\mu = 0$, as opposed to using constant times, which can lead to spurious energies. Another study has recently optimized the rodeo algorithm by using specified times rather than random times [15].

By utilizing the derived expressions, we have estimated various parameters to characterize the peaks efficiently, optimizing the rodeo circuit. We have also derived expressions for the uncertainty caused by the random times we consider in the circuit. We have investigated how these parameters depend on the number of cycles N_C and the number of times the probability is averaged, N_{av}. Finally, based on the calculated parameters and their uncertainty, we have estimated the minimum requirements for finding eigenenergies in the rodeo circuit. These requirements include achieving a minimum amplitude P_{min} and being able to distinguish eigenenergies with a minimum resolution δE_{min}.

We have applied the algorithm for a Hamiltonian for the nucleus ^{6}Li using the Cohen-Kurath interaction in the p shell, where we have considered any state and different values as requirements to find both the eigenenergies and the amplitudes and compared them to the real values. We have noticed that, when dealing with random numbers, sometimes we did not get the expected results, however, we did the majority of the time we used the algorithm. In this way, to guarantee to find our eigenenergies together with the amplitudes of any state, we should make the algorithm go through more than once, to discard the peaks that only appear on occasion, being peaks that do not correspond to any eigenenergy.

When dealing with quantum states that have small amplitudes, it is generally necessary to increase the number of rodeo cycles in order to detect the corresponding eigenenergies. However, an alternative approach to consider is using the rodeo algorithm for quantum states with different components, this is, different reference state. In such cases, the amplitudes that might be very small in one state could be relatively larger in other states. By exploiting this property, it may be possible

to detect all the eigenenergies and probabilities without requiring an excessively large number of rodeo cycles, thereby reducing the computational effort needed for the calculations. Another extension is to study more complex nuclei that require Hamiltonian of higher dimensions of 10×10.

Absolutely, running the rodeo circuit on a quantum computer is the crucial next step to validate the algorithm and verify its performance. By executing the algorithm on a quantum computer, we can directly observe the probabilities to obtain $|1\rangle$ in the ancilla qubits and extract the eigenenergies and probabilities of the desired states. Comparing the quantum computation results with the expected values obtained from the classical simulations will allow us to assess the accuracy and reliability of the rodeo algorithm in a real quantum computing environment. This validation is essential to ensure the algorithm's effectiveness and to gain confidence in its practical implementation for solving quantum eigenvalue problems.

Acknowledgements

I would like to express my sincere gratitude to my advisors, Antonio Márquez, Javier Menéndez, and Arnau Rios, for their invaluable guidance and assistance throughout this work. Their expertise and support have been instrumental in shaping this research. I am also grateful to my family for their encouragement and understanding during this journey.

Bibliography

1. Nielsen, M. A. & Chuang, I. L. *Quantum Computation and Quantum Information: 10th Anniversary Edition* 10th. ISBN: 1107002176 (Cambridge University Press, USA, 2011).

2. Peruzzo, A. *et al.* A variational eigenvalue solver on a photonic quantum processor. *Nature Communications* **5.** https://doi.org/10.1038%2Fncomms5213 (July 2014).

3. Tilly, J. *et al.* The Variational Quantum Eigensolver: A review of methods and best practices. *Physics Reports* **986,** 1–128. https://doi.org/10.1016%2Fj.physrep.2022.08.003 (Nov. 2022).

4. Stetcu, I., Baroni, A. & Carlson, J. Variational approaches to constructing the many-body nuclear ground state for quantum computing. *Phys. Rev. C* **105,** 064308. https://link.aps.org/doi/10.1103/PhysRevC.105.064308 (6 June 2022).

5. Sarma, C., Matteo, O. D., Abhishek, A. & Srivastava, P. C. *Prediction of the neutron drip line in oxygen isotopes using quantum computation* 2023. arXiv: 2306.06432 [nucl-th].

6. Romero, A. M., Engel, J., Tang, H. L. & Economou, S. E. Solving nuclear structure problems with the adaptive variational quantum algorithm. *Phys. Rev. C* **105,** 064317. https://link.aps.org/doi/10.1103/PhysRevC.105.064317 (6 June 2022).

7. Kiss, O. *et al.* Quantum computing of the nucleus via ordered unitary coupled clusters. *Physical Review C* **106.** https://doi.org/10.1103%2Fphysrevc.106.034325 (Sept. 2022).

8. Choi, K., Lee, D., Bonitati, J., Qian, Z. & Watkins, J. Rodeo Algorithm for Quantum Computing. *Phys. Rev. Lett.* **127,** 040505. https://link.aps.org/doi/10.1103/PhysRevLett.127.040505 (4 July 2021).

9. Caurier, E., Martı nez-Pinedo, G., Nowacki, F., Poves, A. & Zuker, A. P. The shell model as a unified view of nuclear structure. *Reviews of Modern Physics* **77,** 427–488. https://doi.org/10.1103%2Frevmodphys.77.427 (June 2005).

10. Lu, S., Bañ uls, M. C. & Cirac, J. I. Algorithms for Quantum Simulation at Finite Energies. *PRX Quantum* **2.** https://doi.org/10.1103%2Fprxquantum.2.020321 (May 2021).

11. Bee-Lindgren, M. *et al. Rodeo Algorithm with Controlled Reversal Gates* 2022. arXiv: 2208.13557 [quant-ph].

12. Varga, R. *Geršgorin and His Circles* ISBN: 9783540211006. https://books.google.es/books?id=q4g0sMe3Ss8C (Springer Berlin Heidelberg, 2011).

13. Cohen, S. & Kurath, D. Effective interactions for the 1p shell. *Nuclear Physics* **73,** 1–24. ISSN: 0029-5582. https://www.sciencedirect.com/science/article/pii/0029558265901483 (1965).

14. Poves, A. & Nowacki, F. in *An Advanced Course in Modern Nuclear Physics* (eds Arias, J. M. & Lozano, M.) 70–101 (Springer Berlin Heidelberg, Berlin, Heidelberg, 2001). ISBN: 978-3-540-44620-0. https://doi.org/10.1007/3-540-44620-6_3.

15. Cohen, T. D. & Oh, H. *Optimizing rodeo projection* 2023. arXiv: 2305.19952 [quant-ph].